Memoirs of the School of Engineering, Nagoya University
Vol.50, No.1/2 (1998)

MICRO FABRICATION BY UV LASER PHOTOPOLYMERIZATION

Katsumi YAMAGUCHI and Takeshi NAKAMOTO

Department of Mechanical Engineering

(Received November 4, 1998)

Abstract

This research deals with the development of simple and practical methods for manufacturing high aspect ratio (height/width) micro parts and three-dimensional micro parts. The first method is mask-based method in which an image is transferred to a liquid photopolymer by irradiating a UV laser through a patterned mask. The irradiated portion of the photopolymer is then solidified and it becomes a high aspect ratio polymer structure or mold. In the second and third methods, high aspect ratio polymer structures are produced using a shaped UV laser beam writing and a focused UV laser beam writing, respectively. The desired product shape is obtained by writing along the contour of the product on the surface of a liquid photopolymer. The written pattern then becomes solid so as to produce a solidified polymer structure or mold. The fourth, three-dimensional micro part is produced by a focused UV laser beam writing method. The accuracy of the solidified polymer when using these methods is examined. The examination is done theoretically and experimentally. The optimum conditions to produce high aspect ratio micro parts and three-dimensional micro parts are also verified. Various shapes of micro polymer structures are produced using these methods.

Keywords: Micro fabrication, Photopolymer, UV laser, High aspect ratio micro part, Three-dimensional micro part, Accuracy, Mask-based method, Beam writing method, Diffraction of light, Absorption of light, Solidification

Contents

1. Mask-Based Method

1.1 Introduction

The manufacture of micro mechanical parts has drawn great attention in recent years at both research and development levels. The manufacturing of micro link and micro sliding mechanisms was a part of the pioneer research work done at AT&T Bell Laboratories[1)] and University of California, Berkeley[2)]. The work was carried out by applying a lithography technique on a semiconductor material. The application of this method led to the manufacture of electro-static motors[3)] and various sensors[4,5)].

The material used to manufacture these micro mechanical parts is silicon, and part thickness of only a few micrometers are possible. Considering the thickness limitation and alternative material properties with further expanded applications, thick metallic micromechanical parts may be desirable. Several recent processes have been developed to meet these requirements[6-24)]. The most successful of these processes is the so-called LIGA (Lithograph Galvanoformung und Abformung) process[6-20)]. In this process, a thick (up to several hundred micrometers) photoresist pattern is made with X-rays radiation from a synchrotron. Using the pattern as a mold, a high aspect ratio (height/width) metallic micro mechanical structure is made by an electroforming process. This process is used to produce various micromachined parts such as separation nozzles[12)], X-ray masks[13)] etc. A variation of the LIGA process using sacrificial layer is the so-called SLIGA (Sacrificial-LIGA) process which produces flexible or free rotating microstructures[7,8,14-16)]. The application of this method led to the manufacture of a planar magnetic micromotor[15)] microturbine[7)] etc. The processing sequence produce flanks for which the run-out is less than 0.3 μm in 100 μm height. However, from a practical point of view, synchrotron X-rays pose limitations because of size, expense and availability constraints.

Several recent studies on three dimensional polymer structures and models describe details of direct writing and scanning processes[24-27)]. In these methods, two dimensional polymer structures are made by writing or scanning with a laser beam on the surface of a liquid photopolymer. The irradiated portion of the liquid photopolymer is then solidified. Three dimensional solidified polymer structures are then attained by stacking the polymer layers on top of one another until the desired height is reached. Various studies related to these methods have investigated the equipment and processing steps in more detail. However, micro fabrication and the accuracy of the polymer structures are not clarified in detail when using writing and scanning methods.

Three distinct methods are used to produce micro structures of various sizes and shapes. The first method is mask-based method[28,29)] in which an image is transferred to a liquid photopolymer by irradiating a UV laser through a patterned mask as shown in Fig. 1-1 (a). The irradiated portion of the photopolymer is then solidified. Next, upon development, only the solidified portion becomes a high aspect ratio micro polymer structure or micro mold. In the second method, high aspect ratio solidified polymer structures are produced by using direct writing a shaped UV laser beam[30)] on the surface of a liquid photopolymer along the contour of the products as shown in Fig. 1-1 (b). In the third method, polymer structures are produced by direct writing using a focused UV laser beam[31)] as shown in Fig. 1-1 (c).

In this study, the shapes of the solidified polymer obtained by theoretical calculations are compared with those obtained experimentally. Using the theoretical and experimental results, various micro polymer structures with reasonably high accuracy are made.

This section examines the accuracy of the solidified photopolymer produced by mask-based method. The simulation and results of the experiment on the pattern transfer process are described in detail. The purpose of this section is to manufacture micromachine parts on the order of 0.01–1.0 mm in size in a relatively simple and economical way, compared to the present press forming.

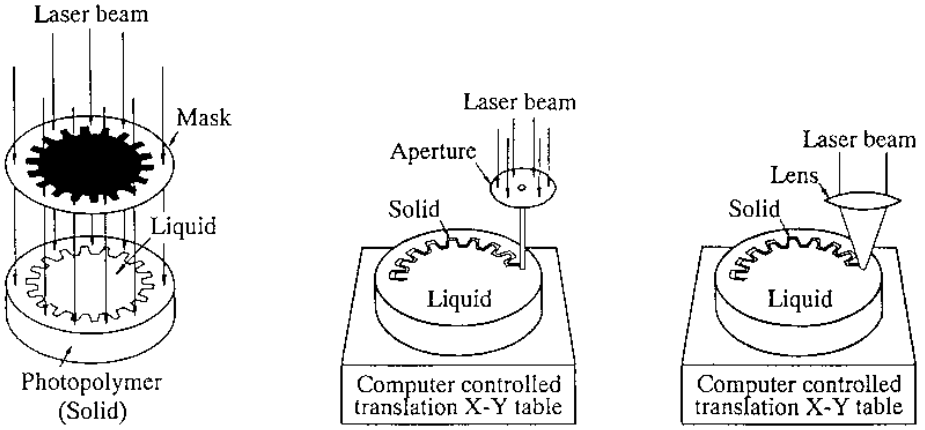

(a) Mask-based pattern transfer (b) Direct shaped beam writing (c) Direct focused beam writing

Fig. 1-1 Fabrication methods of micro structures

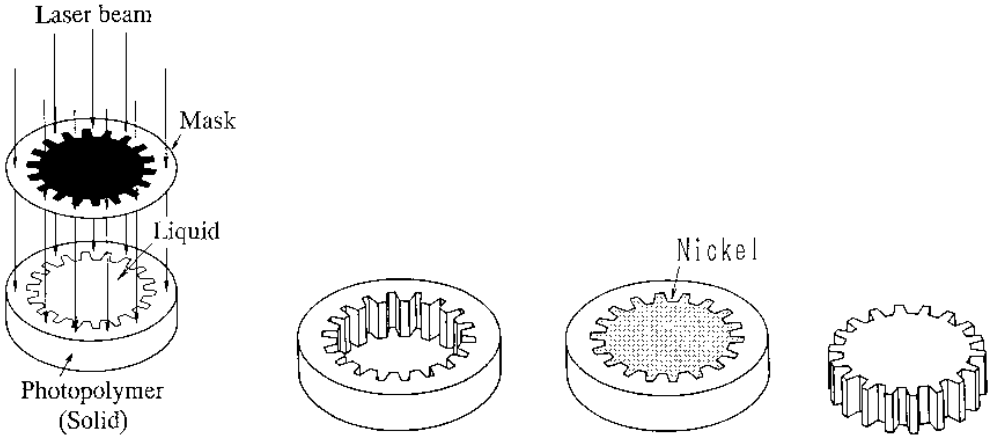

(a) Irradiation (b) Development (c) Electroforming (d) Product

Fig. 1-2 Schematic diagram of mask-based method

1.2 Manufacturing method

Fig. 1-2 shows the manufacturing method employed to produce high aspect ratio micromechanical parts such as a gear. At first, laser beam is irradiated on the surface of the liquid photopolymer passing through the mask as shown in (a). At this time the irradiated portion of the liquid photopolymer becomes solid. Next, upon development, only the solidified portion remains as shown in (b). After the development, materials such as nickel are electroformed into an electrically conducting substrate shown in (c). Finally, upon removing the solidified photopolymer, the metallic gear remains as shown in (d). Fig. 1-2 shows a gear-making process. However, depending on the irradiation, development and electroforming process repetition, a gear shaft assembly could also be made.

1.3 Theoretical analysis of pattern transfer

This section deals with the processes of pattern transfer explained in Fig. 1-2 (a). In order to produce thick and accurate products, the accuracy of the part dimension and the verticality of the side wall along the thickness are essential. The main factors affecting the accuracy are diffraction, absorption and fluorescence. The effect of fluorescence is not significant and is dealt with in Section 1.5.1. In this section, the effect of diffraction and absorption on the accuracy of pattern transfer are examined.

Fig. 1-3 shows the theoretical model used to simulate the shape of the solidified polymer. Fig. 1-3 (a) shows the theoretical model used when a beam with uniform intensity is irradiated through a square mask onto the surface of the liquid polymer. Here I_o is the beam intensity, λ the wavelength, a the length of the square, and h the distance between the mask and the surface of the polymer. In this experiment, the mask and photopolymer surface distance h is far greater than the wavelength of the light source. Therefore, Fresnel's diffraction theory can be applied to calculate the effect of diffraction. Let the center of the mask be at $x=0$, $y=0$ and the depth of the polymer be along z. The light intensity after diffraction at $I_d(x,y,z)$ can be expressed as follows[32,33].

$$I_d(x,y,z) = \frac{1}{4} I_o \left[C_x^2 C_y^2 + C_x^2 S_y^2 + S_x^2 C_y^2 + S_x^2 S_y^2 \right] \tag{1-1}$$

Where,

$$C_x = \int_{p_1}^{p_2} \cos\left(\frac{1}{2}\pi u^2 \right) du \tag{1-2}$$

$$S_x = \int_{p_1}^{p_2} \sin\left(\frac{1}{2}\pi u^2 \right) du \tag{1-3}$$

$$C_y = \int_{q_1}^{q_2} \cos\left(\frac{1}{2}\pi u^2 \right) du \tag{1-4}$$

$$S_y = \int_{q_1}^{q_2} \sin\left(\frac{1}{2}\pi u^2 \right) du \tag{1-5}$$

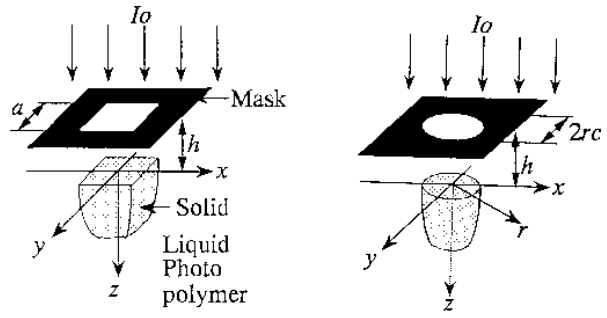

(a) Square beam (b) Circular beam

Fig. 1-3 Theoretical model

$$p_1 = \frac{2}{\sqrt{m}}\left(\frac{x}{a} - \frac{1}{2}\right) \tag{1-6}$$

$$p_2 = \frac{2}{\sqrt{m}}\left(\frac{x}{a} + \frac{1}{2}\right) \tag{1-7}$$

$$q_1 = \frac{2}{\sqrt{m}}\left(\frac{y}{a} - \frac{1}{2}\right) \tag{1-8}$$

$$q_2 = \frac{2}{\sqrt{m}}\left(\frac{y}{a} + \frac{1}{2}\right) \tag{1-9}$$

$$m = \frac{2\lambda(h+z)}{a^2} \tag{1-10}$$

In these equations C_x, S_x, C_y and S_y are Fresnel's integrals.

When a beam is irradiated through a circular mask with a radius r_c, as shown in Fig. 1-3 (b), I_d can be expressed as follows[32,33].

$$I_d(r,z) = \frac{4\pi^2 I_o}{\lambda^2 (h+z)^2} \times \left\{ \left[\int_0^{r_c} \cos\left(\frac{\pi\rho^2}{\lambda(h+z)}\right) J_o\left(\frac{2\pi\rho r}{\lambda(h+z)}\right) \rho \, d\rho \right]^2 + \left[\int_0^{r_c} \cos\left(\frac{\pi\rho^2}{\lambda(h+z)}\right) J_o\left(\frac{2\pi\rho r}{\lambda(h+z)}\right) \rho \, d\rho \right]^2 \right\} \tag{1-11}$$

The integrals in equation (1-11) are Fresnel's integral as expressed in the cylindrical coordinate, and J_o is the 0 order type 1 Bessel function.

The intensity of the diffracted light decreases due to absorption of the light by the photopolymer. Let the absorption coefficient of the photopolymer for the incident light be α. The relationship between the absorption coefficient and light intensity at depth z, denoted as I, can be expressed as follows:

$$I(x,y,z) = I_d \cdot \exp(-\alpha z) \tag{1-12}$$

The irradiated energy per unit area, E, at (x,y,z) having been irradiated for the period of time t, can be expressed as follows.

$$E(x, y, z, t) = I(x, y, z) \cdot t \tag{1-13}$$

When the irradiated energy $E(x,y,z)$ attains the threshold value E_o, the photopolymer is assumed to solidify. Therefore (x,y,z) satisfying equation (1-14) becomes the shape of the solidified polymer.

$$I(x, y, z) = \frac{E_o}{t} \tag{1-14}$$

Preliminary test were done to determine the value of α and E_o. When the incident light has the uniform intensity I_o, the depth of solidified photopolymer z, can be expressed as follows[34].

$$z = \frac{1}{\alpha} \log_e \left(\frac{I_o \cdot t}{E_o} \right) = \frac{1}{\alpha} \log_e \left(\frac{t}{t_o} \right) \tag{1-15}$$

$$E_o = I_o \cdot t_o \tag{1-16}$$

The photopolymer surface layer starts to solidify for the period of time t_o. The value of α, E_o and t_o can be obtained from the relationship between the exposure time and the depth of the solidified photopolymer. These results are illustrated in Fig. 1-4. The values obtained on the basis of the figure are $\alpha = 6.94 \times 10^{-3}$ (1/μm), $t_o = 1.06$ seconds and $E_o = 0.34$ mJ/mm^2.

Fig. 1-5 shows a simulation of the shape of the solidified polymer obtained when using a mask with the square and circular cross sections shown in (a) and (b), respectively. In these figures, the solidified polymer is shown upside down for clarity. The simulations show that both the square and circular patterns form slightly tapered walls, though straight walls are desirable to make precise molds as shown in Fig. 1-2.

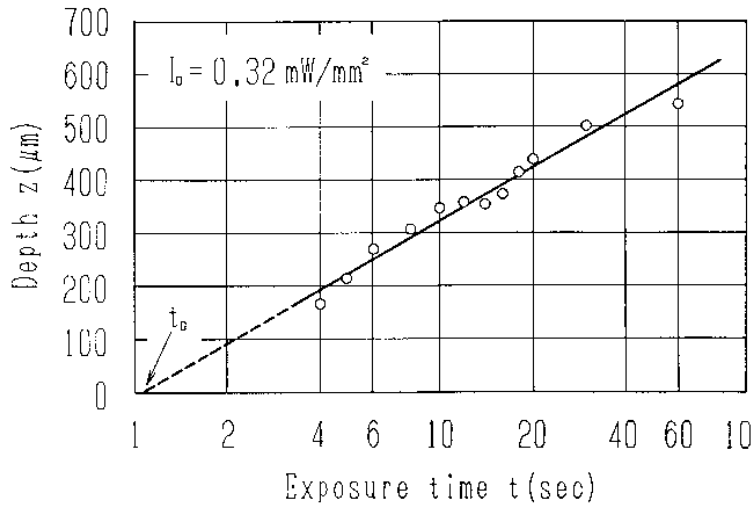

Fig. 1-4 Experimental data obtained from the relationship between the exposure time and depth of the solidified photopolymer

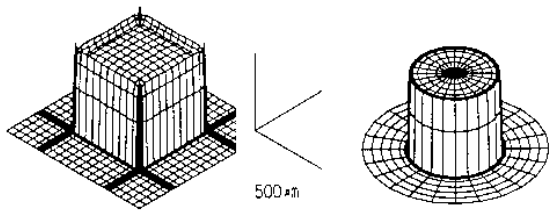

(a) Square beam [a = 500 μm] (b) Circular beam [r_c = 250 μm]

Fig. 1-5 Simulation of the solidified polymer shape [I_o = 1 mW/mm^2, λ = 0.325 μm, h = 10 μm, $\alpha = 6.94 \times 10^{-3}$ (1/μm), t = 10 sec]

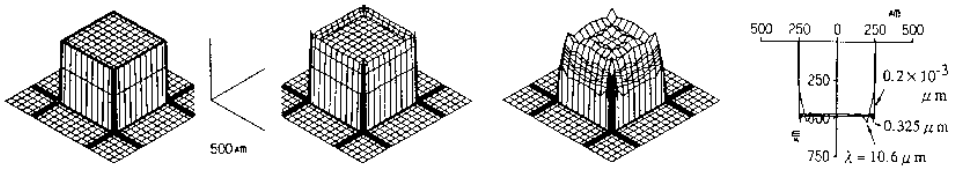

(a) $\lambda = 0.2 \times 10^{-3}$ μm (b) λ = 0.325 μm (c) λ = 10.6 μm (d) Comparison of the cross sections

Fig. 1-6 Simulation of the solidified polymer shape [I_o = 1 mW/mm^2, a = 500 μm, h = 10 μm, $\alpha = 6.94 \times 10^{-3}$ (1/μm), t = 10 sec]

1.4 The effect of the physical parameters

This section examines the effect of the physical parameters such as wavelength λ, absorption coefficient α, and the mask-polymer distance h, on the accuracy of the solidified polymer layer obtained when transferring mask patterns. As an example, a mask with a square cross section is used.

1.4.1 Wavelength, λ

Fig. 1-6 (a), (b) and (c) show results of simulating the shape of the solidified polymer when the wavelength, λ, of the irradiated beam is 0.2×10^{-3} μm, 0.325 μm and 10.6 μm for SOR (LIGA process), He-Cd laser (present research experimental apparatus) and CO_2 laser (not practical but included for reference), respectively. Fig. 1-6 (d) presents a comparison of the cross sections of the solidified polymer when varying the wavelength, λ. The figure indicates that the wavelength affects the accuracy of the pattern transfer. The production errors of the width at 100 μm depth are 0.07 μm, 3 μm and 16 μm for $\lambda = 0.2 \times 10^{-3}$ μm, 0.325 μm and 10.6 μm, respectively.

1.4.2 Mask-polymer surface distance, h

Fig. 1-7 (a), (b) and (c) show simulations of the shape of the solidified polymer when the value of the mask-polymer surface distance, h, is 10 μm, 1000 μm and 100000 μm (not practical but included for reference), respectively. Fig. 1-7 (d) presents a comparison of the cross sections when varying the mask-polymer surface distance, h. The smaller the mask-polymer surface dis-

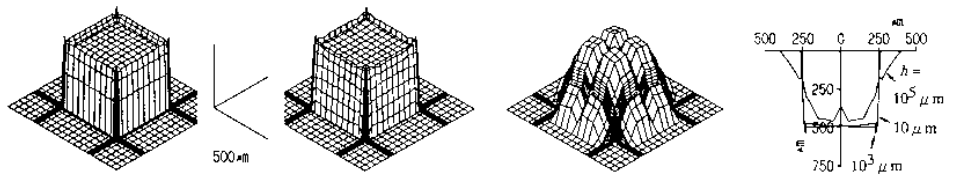

(a) h = 10 μm (b) h = 1000 μm (c) h = 100000 μm (d) Comparison of the cross sections

Fig. 1-7 Simulation of the solidified polymer shape
[I_o = 1 mW/mm^2, a = 500 μm, λ = 0.325 μm, $\alpha = 6.94 \times 10^{-3}$ (1/μm), t = 10 sec]

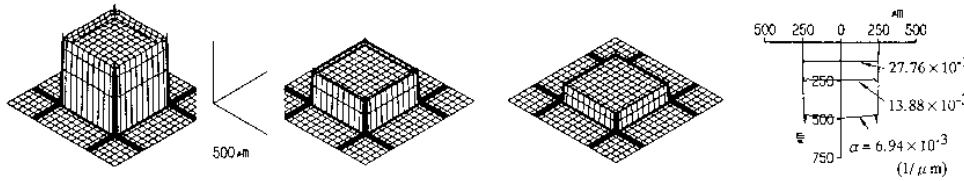

(a) $\alpha = 0.694 \times 10^{-3}$ (1/μm) (b) $\alpha = 13.88 \times 10^{-3}$ (1/μm) (c) $\alpha = 27.76 \times 10^{-3}$ (1/μm) (d) Comparison of the cross sections

Fig. 1-8 Simulation of the solidified polymer shape
[I_o = 1 mW/mm^2, a = 500 μm, λ= 0.325 μm, h = 10 μm, t = 10 sec]

tance, the higher the accuracy of the pattern transfer. The production errors of the width at 100 μm depth are 3 μm, 10 μm and 111 μm for h = 10 μm, 1000 μm and 100000 μm, respectively.

1.4.3 Absorption coefficient, α

Fig. 1-8 (a), (b) and (c) show simulations of the shape of the solidified polymer when the value of the absorption coefficient, α, is 6.94×10^{-3} (1/μm), 13.88×10^{-3} (1/μm) and 27.76×10^{-3} (1/μm), respectively. The values correspond to 2 and 4 times the absorption coefficient of the experimental polymer (6.94×10^{-3} (1/μm)).

Fig. 1-8 (d) presents a comparison of the cross sections when varying the absorption coefficient, α. The production errors of the width at 100 μm depth are almost the same for the absorption coefficients shown in Fig. 1-8 (d). However, the larger the absorption coefficient becomes, the more irradiating time is necessary so as to achieve the same solidified depth. Therefore the solidified width becomes greater at the surface of the polymer. The production errors become 1 μm, 2 μm and 4 μm for $\alpha = 6.94 \times 10^{-3}$ (1/μm), 13.88×10^{-3} (1/μm), 27.76×10^{-3} (1/μm), respectively, at the optimum irradiating time.

When the mask-polymer surface distance h = 10 μm, the absorption coefficient $\alpha = 6.94 \times 10^{-3}$ (1/μm) and the optimum irradiating time t = 2.1 sec, the production error of the width at 100 μm depth are 0.03 μm, 1 μm for $\lambda = 0.2 \times 10^{-3}$ μm (SOR) and 0.325 μm (UV laser), respectively.

1.4.4 Optimum condition for UV laser and present photopolymer

The light source is a He-Cd Laser (wavelength 325 nm) in this experiment. And the absorption coefficient of photopolymer used in this experiment is 6.94×10^{-3} (1/μm) described in Sec. 1.3. Fig. 1-9 (a) shows a simulation of the solidified polymer in this condition. In this figure, the

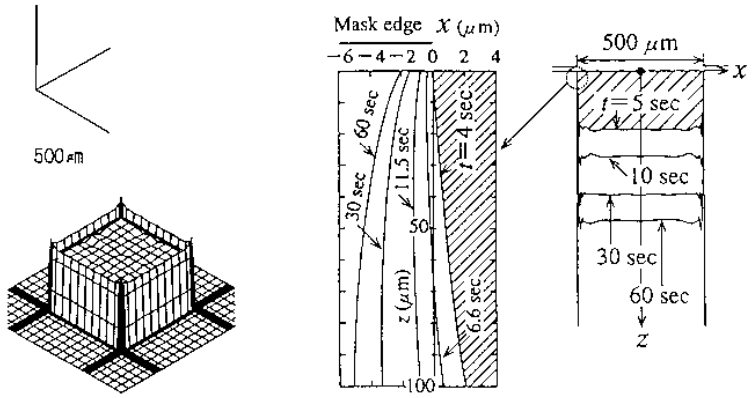

(a) Solidified polymer shape [t = 10 sec] (b) Cross section

Fig. 1-9 Simulation of the shape of the solidified photopolyer
[I_o = 0.32 mW/mm^2, a = 500 μm, h = 10 μm]

solidified polymer is shown upside down for clarity. The right of Fig. 1-9 (b) shows a simulation of the shape of the cross section of the solidified polymer. As can be seen from the figure, as the irradiation time increases, the depth and width of the solidified polymer increase. The increment in the width is very small and gradual as compared to the depth of the solidified polymer. The left of the Fig. 1-9 (b) shows the sidewall of the solidified polymer. In order to readily distinguish the solidified shape, the x coordinate is magnified to 5 times that of the z coordinate. When the photopolymer is solidified at the ideal condition of t = 6.6 seconds and depth of 100 μm, straight edge pattern transfer accuracy of ±0.5 μm is possible. Hence, for the both sides, the accuracy of pattern transfer is ±1 μm.

1.5 Experiment on pattern transfer process

1.5.1 Experimental photopolymer

The photopolymer used in this experiment is a product of Asahi Chemical Co., Ltd. The photopolymer material is an unsaturated polyester. The trade name is APR stamp resin (Katadori-20). This photopolymer is usually used for plate-making in the printing technology. The photopolymer has a maximum sensitivity at a wavelength of 365 nm.

Fig. 1-10 shows the absorption characteristics of the photopolymer versus the wavelength. The absorption coefficient of the solid is larger than that of the liquid and the larger the wavelength the better the transmittance. The irradiating light wavelength 325 nm which is used in this experiment was shown to be transmitted sufficiently in both liquid (before solidification) and solid (after solidification) photopolymer.

The fluorescence spectral analysis shows that the peak of the fluorescence spectrum is 390 nm and 400 nm before and after solidification, respectively. The intensity of the light due to the effect of fluorescence is very weak compared to the intensity of the incident light. Therefore, the effect of the fluorescence is negligible compared to that of diffraction and absorption.

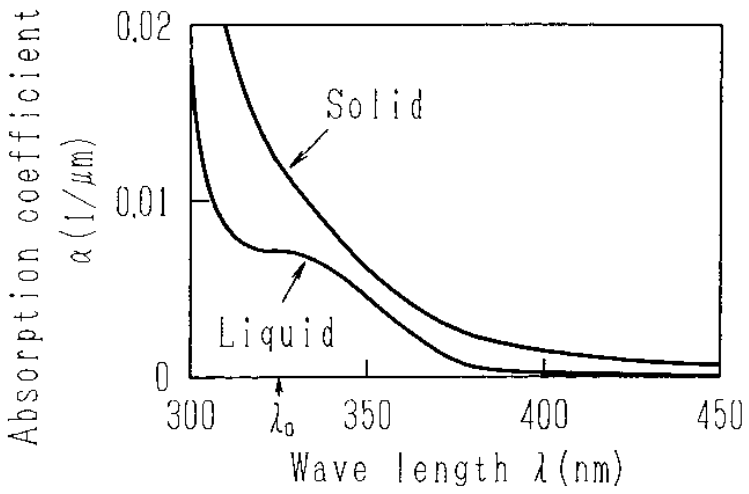

Fig. 1-10 The absorption characteristics of the photopolymer versus the wavelength

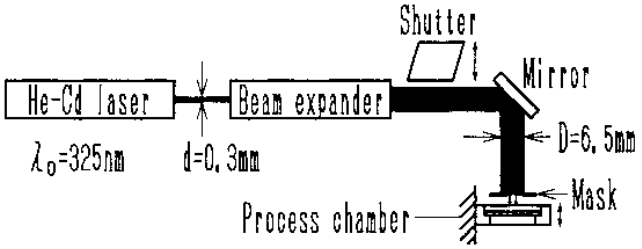

Fig. 1-11 Schematic layout of the experimental setup

1.5.2 Experimental method

Fig. 1-11 shows the schematic layout of the experimental setup. The light source is a He-Cd Laser (wavelength 325 nm, 10 mW continuous Gaussian beam). This wavelength is close to that which solidifies the photopolymer. A beam expander is used to produce a broad beam enabling the central flat portion of the intensity distribution to be used. This broad beam is irradiated onto the photopolymer surface through a mask.

The liquid photopolymer is uniformly smeared onto the surface of a quartz substrate. After a holding time of 1 minute the liquid photopolymer settles, after which it is irradiated by the laser beam. The photopolymer is then developed for 90 seconds using acetone. The solidified photopolymer is observed by an optical microscope.

1.6 Comparison of theoretical and experimental results

Fig. 1-12 (a) shows a solidified portion in the liquid polymer. The photograph gives a cross-sectional view of the solidified shape. Here the beam is irradiated from the upper side. Fig. 1-12 (b) shows the simulated shape. Comparison of the simulation and experimental results reveals similar shapes. Because the end portion of the polymer is not completely solidified, it is not visible in

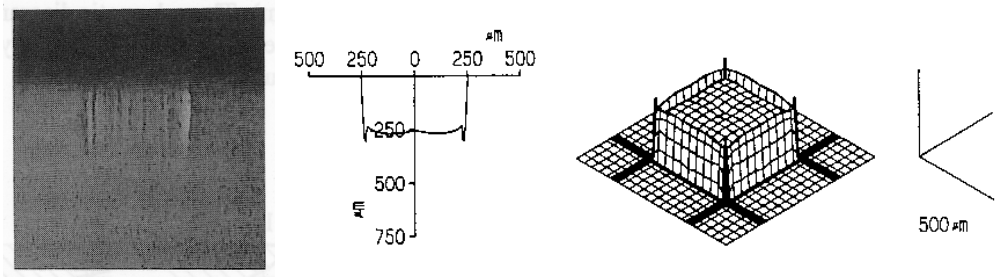

(a) Experimental shape (b) Simulation of the cross section (c) Simulation of the solidified polymer

Fig. 1-12 Comparison of experimental shapes and simulation of solidifed polymer
[I_o = 0.31 mW/mm^2, a = 500 μm, λ = 0.325 μm, h = 1000 μm, $\alpha = 6.94 \times 10^{-3}$ (1/μm), t = 7 sec]

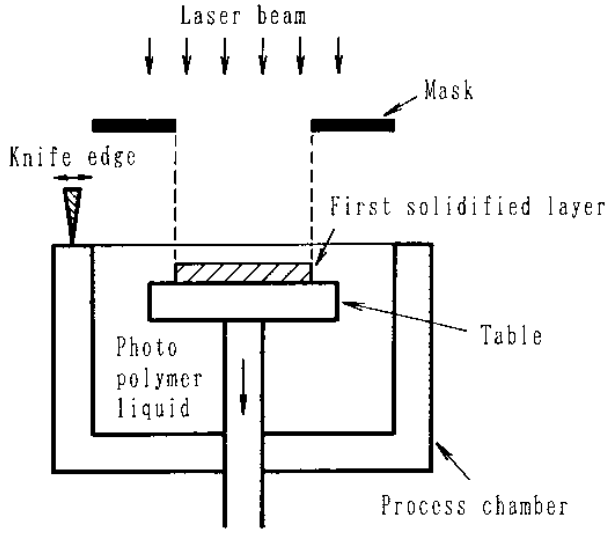

Fig. 1-13 Apparatus for stacking procedure

(a). Fig. 1-12 (c) shows the simulation of the solidified polymer. In this figure the solidified polymer is shown upside down for clarity.

Next, upon development, only the solidified portion remains. Because the end of the polymer is not completely solidified, the developer dissolves the polymer more easily there; and the edge shape of the solidified polymer becomes smooth by the surface tension. However, only the solidified sidewalls are used in making a high aspect ratio micro-mold as shown in Fig. 1-2. Therefore the shape of the end of the solidified polymer is not important.

1.7 The manufacturing of high aspect ratio products

The maximum depth of solidification for which we can expect a reasonably high accuracy is about 100 μm. Beyond this limit the accuracy decreases. However, if a thicker wall is desired, the

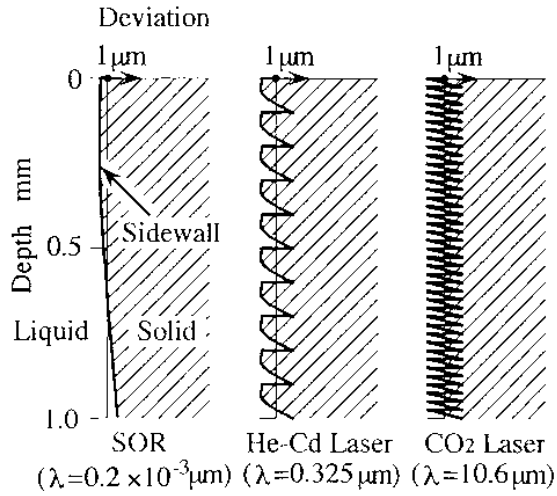

Fig. 1-14 Schematic diagrams of the simulation of the stacking method for various wavelengths
[$h = 10\ \mu$m, $\alpha = 6.94 \times 10^{-3}$ (1/μm)]

following procedure is adopted.

Fig. 1-13 shows the apparatus for this procedure. First, the liquid photopolymer is poured into the process chamber with a depth of 100 μm. The first layer of the solidified photopolymer is then made by irradiation. Next, the table is moved 100 μm downwards and an equal amount of liquid film is spread on top of the solidified layer. The second layer is solidified by a second exposure and so on. After this stacking procedure is completed, the photopolymer is developed. Following this method, a high aspect ratio of reasonably high accuracy can be obtained.

In order to obtain a 1 μm accuracy at a depth of 1000 μm, the number of polymer layers required when using $\lambda = 0.2 \times 10^{-3}\ \mu$m, 0.325 μm and 10.6 μm is 1, 10 and 40 layers, respectively. The simulations are done using the values of $h = 10\ \mu$m and $\alpha = 6.94 \times 10^{-3}$ (1/μm). The schematic diagrams of simulations of the sidewall produced by the stacking method for various wavelength are shown in Fig. 1-14.

Fig. 1-15 shows the scanning micrograph of the solidified photopolymer produced by the stacking method. The sidewall profiles of the micro-mold produced by the stacking method are measured by stylus instrument as shown Fig. 1-16. The left shows the simulation profile and the right shows the experimental profile.

The smaller the distance h, the smaller the increment in the width of the solidified polymer. For $h = 10\ \mu$m, the simulation shows a productive error of 1 μm. An error of 1 μm, however, is difficult to measure. Therefore a large distance h which results in a larger productive error (measurable) facilitates comparison of the simulation and experimental profile. The distance is thus kept at $h = 1000\ \mu$m. The thickness of one layer is 100 μm.

The simulation and experimental profiles of the sidewalls have the surface waviness of 6 μm and 8 μm, respectively. The sidewall profiles of both simulation and experimental match closely.

Fig. 1-17 shows some example of a photopolymer mold obtained by the stacking method. Fig. 1-18 (a) and (b) indicate examples of a mold obtained by a single and two alternate masks, respectively.

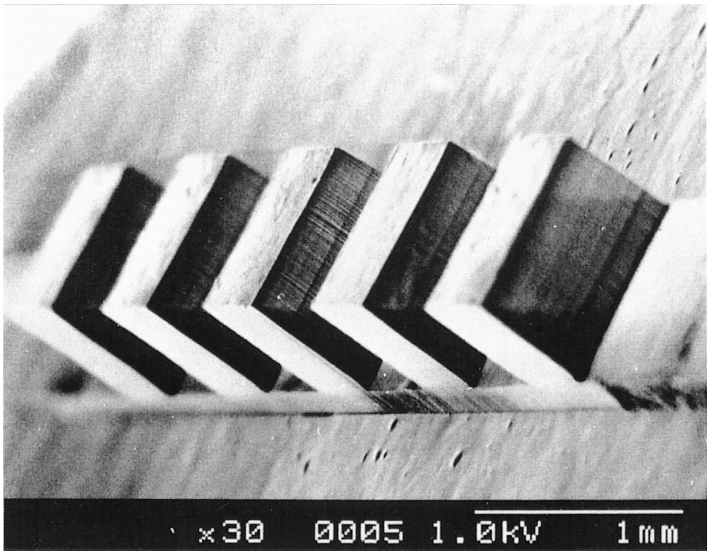

Fig. 1-15 Scanning micrograph of the solidified photopolymer produced by the stacking method

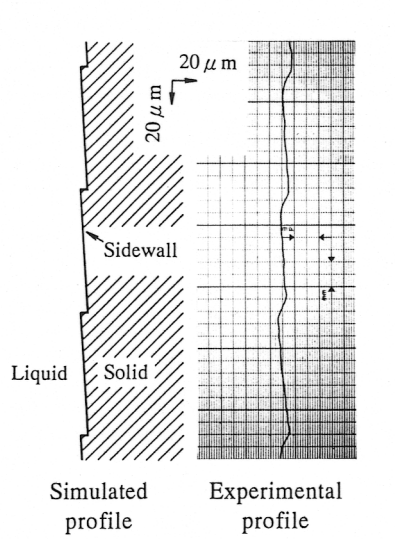

Fig. 1-16 Sidewall profiles of the micro polymer structure
[I_o = 0.32 mW/mm^2, a = 500 μm, h = 1000 μm, t = 7 sec]

1.8 Conclusions

Based on the theoretical analysis and experimental results of the mask-based method, the following conclusions can be obtained.

(1) The shape and accuracy of the solidified photopolymer are estimated using both Fresnel's

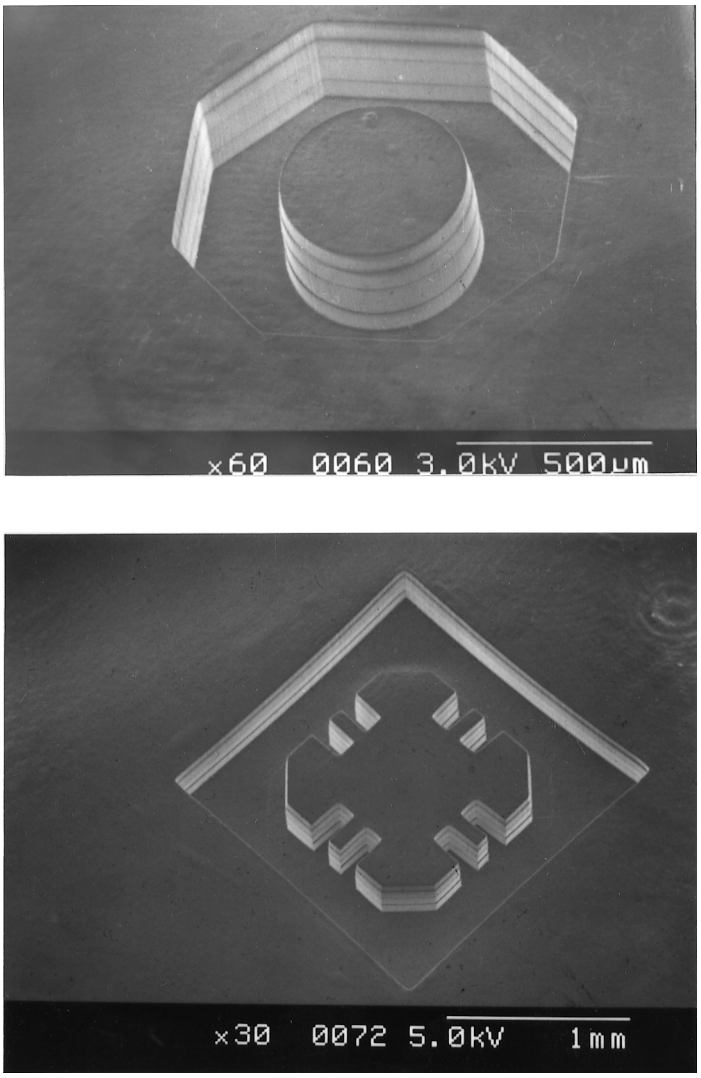

Fig. 1-17 Examples of photopolymer mold obtained by the stacking method

diffraction theory and the theoretical considerations reached for the absorption of light.

(2) The effect of the physical parameters on the shape and accuracy of the pattern transfer can be examined by simulation.

(3) In proximity transfer, for a depth of 100 μm, an accuracy of 0.03 μm and 1 μm can be expected from simulation using an SOR and UV laser source, respectively.

(4) Using a UV laser and the stacking method, thick and high aspect ratio microstructures with the sidewall surface waviness of 8 μm can be produced.

(5) According to the theoretical analysis, an accuracy of ±1 μm could be attained when the distance between the mask and the surface of the photopolymer is 10 μm.

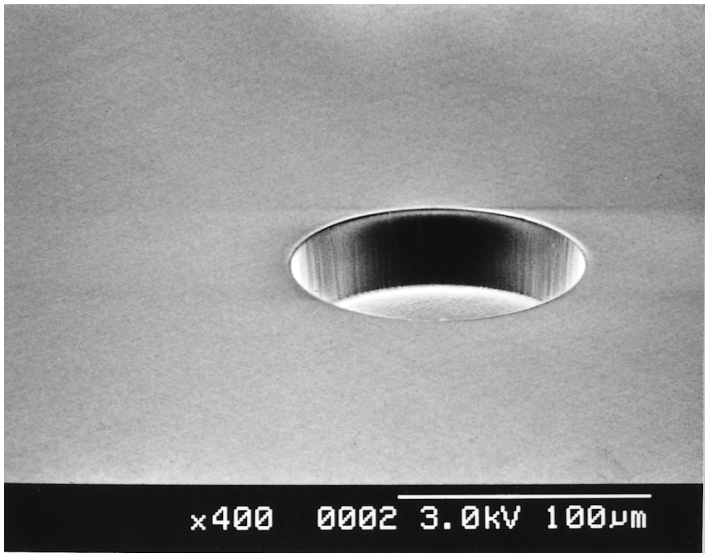

(a) Photopolymer mold obtained by a single mask

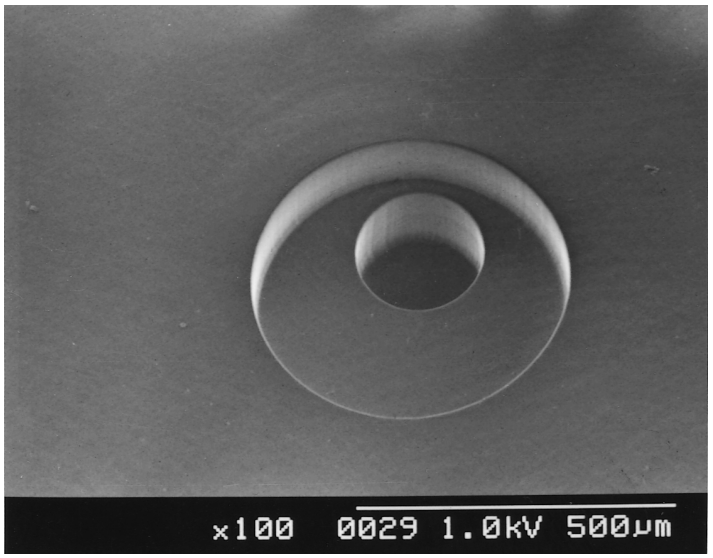

(b) Photopolymer mold obtained by two alternate masks

Fig. 1-18 Examples of photopolymer mold obtained by a single mask and two alternate masks

2. Writing Method

2.1 Introduction

Several recent studies on three dimensional polymer structures and models describe details of maskless fabrication processes[24-27,30,31,35-37]. Writing and scanning methods are maskless direct beam processes that provide a great deal of flexibility in designing various patterns. This is especially beneficial when lower production volume is desired. In the scanning method, a focused beam is manipulated by various deflecting devices such as in galvanometer-type scanners[26], polygon scanners[27] and acousto-optical scanners[36]. The desired product shape is obtained by scanning the entire area using controlled exposure.

Direct writing along the contour of the product using a shaped beam is another method used[37]. In this method, various apertures are employed to shape the beam with the desired contour obtained by moving an X-Y table. In direct writing and scanning processes, when the polymer is irradiated, only two dimensional structures can be obtained. Three dimensional structures are then attained by stacking the polymer layers on top of one another until the desired height is reached.

The purpose of this research is to manufacture high aspect ratio precision micro-molds by the direct writing method. Various studies related to three dimensional microfabrication on polymer layers using direct writing and scanning methods have investigated the equipment and processing steps in more detail[24-27,36,37]. The effects of using various shaped beams on the lateral dimensions and verticality of the sidewalls when using the scanning and writing methods however, have not been clarified in detail.

Here we examine the shape of the solidified polymer produced by direct laser writing using various shaped beams and intensity distributions along commonly used contours. The examination is done both theoretically and experimentally. The shapes obtained by theoretical calculations are compared with those obtained experimentally. The intensity distribution of irradiated beams and the kind of shaped beam which is effective in making combinations of various contours are verified in detail. Using the theoretical and experimental results, various high aspect ratio micro-molds and polymer structures with reasonably high accuracy are made.

2.2 Manufacturing method

In this study, the manufacture of polymer structures or models is done by direct writing on the surface of the polymer which is then developed with a highly selective developer. Fig. 2-1 (a) shows a schematic diagram of the manufacturing method to produce micromechanical parts such as a gear by direct laser writing on the surface of a liquid polymer along the gear contour. During this process, a gear is obtained as shown in (b) by writing on the inner side of the contour. When writing on the outer side, a mold is obtained as shown in (c). Further mold filling processes produce products from metals, plastics, and ceramics. The most common of these processes is electroforming, in which nickel or copper material is deposited into a polymer mold.

The dimensional accuracy of the product is determined by the precision of the lateral dimensions and the verticality of the sidewalls along the thickness. The width of the solidified polymer along the thickness is affected by the shape and intensity distribution of the irradiated beam as well as diffraction and absorption of light within the polymer[28]. This paper examines the shape of the solidified polymer when writing with different beam shapes and intensity distributions along commonly used contours. The verticality of the sidewalls is examined considering the theories of diffraction and absorption of light.

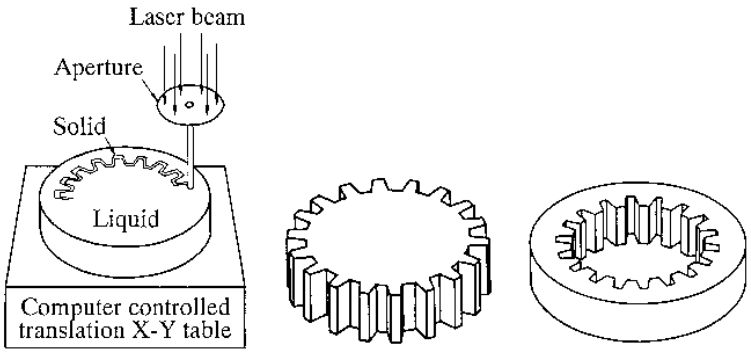

(a) Direct laser writing (b) Polymer structure (c) Mold

Fig. 2-1 Schematic diagram of the manufacturing method

2.3 Analysis of the shape of the solidified polymer

2.3.1 Simulation

The verticality of the sidewalls is examined considering the theories of diffraction and absorption of light. Beams of uniform intensity having a square and a circular cross section (called square and circular beams, respectively, hereinafter) and a gaussian beam are used. Consider a square or circular beam, the light intensity after diffraction through a aperture and absorption in a photopolymer I at (x,y,z), can be expressed as equation (1-12). For a beam with a gaussian intensity distribution, the light intensity of the beam after absorption in a polymer is expressed as follows.

$$I(r,z) = 2\,I_o \cdot \exp\left(-\frac{2r^2}{r_o^2}\right) \cdot \exp(-\alpha \cdot z) \tag{2-1}$$

Here r_o is a gaussian radius and I_o is the mean intensity within radius r_o.

When writing along a straight line (x-axis) at a constant speed, v, the irradiated energy per unit area, E, at (x,y,z) can be expressed as follows.

$$E(x,y,z) = \int_{-\infty}^{+\infty} I(x - v\,t, y, z)\,dt \tag{2-2}$$

When the irradiated energy $E(x,y,z)$ attains the threshold value E_o, the polymer is assumed to solidify. Therefore, the line (y,z) satisfying equation (2-3) becomes the outline of the solidified polymer.

$$\int_{-\infty}^{+\infty} I(x - v\,t, y, z)\,dt = E_o \tag{2-3}$$

The outline of the solidified polymer is obtained by substituting equations (1-12) or (2-1) into (2-3).

Fig. 2-2, 2-3 and 2-4 give simulations of the shape of the solidified polymer when using a

square, circular, and gaussian beam, respectively. When the laser beam is statically irradiated for 10 seconds, the shape of the solidified polymer becomes that shown in Fig.2-2 (a), 2-3 (a) and 2-4 (a). The beam is irradiated from the bottom side, so the solidified polymer is shown upside down.

When writing along a straight line, the shape of the solidified polymer become that shown in Fig.2-2 (b), 2-3 (b), and 2-4 (b). Cross sectional views of the solidified polymer are shown in Fig.2-2 (c), 2-3 (c) and 2-4 (c). The writing speeds 25, 50 and 100 μm/sec are used for the cross sections

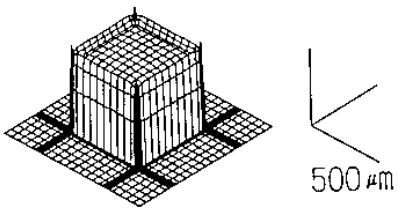

(a) Stationary irradiation [t = 10 sec]

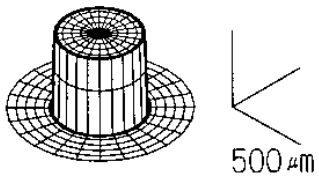

(a) Stationary irradiation [t = 10 sec]

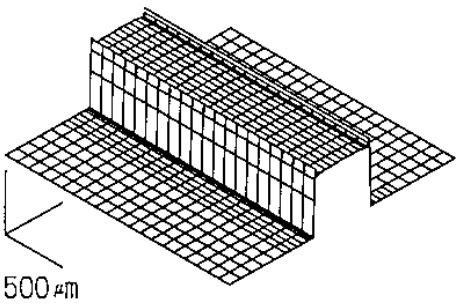

(b) Writing along a straight line [v = 50 μm/sec]

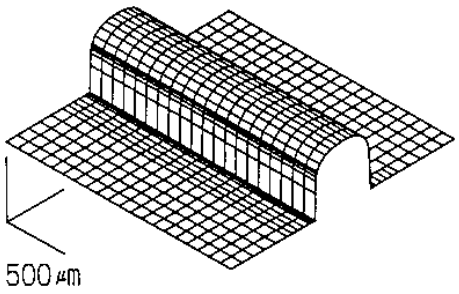

(b) Writing along a straight line [v = 50 μm/sec]

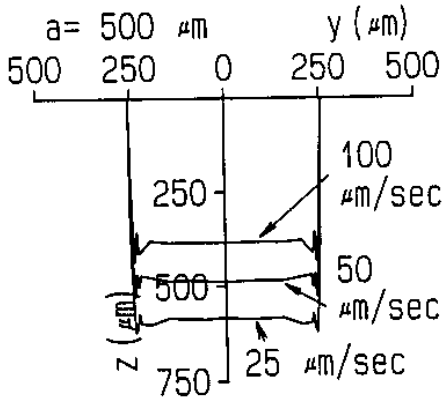

(c) Cross sectional view

Fig. 2-2 Simulation of the shape of the solidified polymer when using a square beam [I_o = 1 mW/mm^2, a = 500 μm, h = 10 μm]

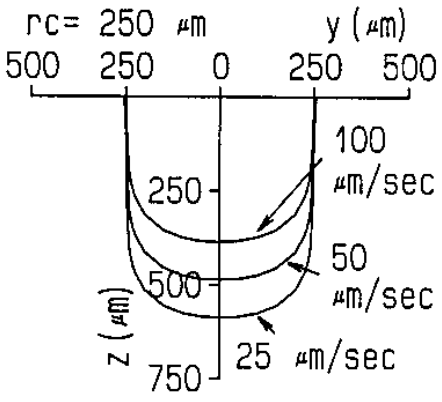

(c) Cross sectional view

Fig. 2-3 Simulation of the shape of the solidified polymer when using a circular beam [I_o = 1 mW/mm^2, r_c = 250 μm, h = 10 μm]

shown. Here the irradiation is from the top side. When the writing speed is changed, the width of the solidified polymer irradiated by a square and circular beam does not change significantly while that irradiated by a gaussian beam does. When the writing speed varies from 25 to 100 μm/sec, the difference in the width measured at the surface is 3 μm and 7 μm for square and circular beam, respectively. The difference becomes 130 μm when a gaussian beam is used. When making high aspect ratio products, a constant width of the solidified polymer along the depth is desirable. When writing at a speed of 25 μm/sec, the difference in the width of the solidified polymer measured at the surface and at a depth of 200 μm is 4 μm and 6 μm for a square and circular beam, respectively.

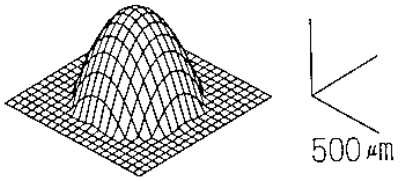

(a) Stationary irradiation [t = 10 sec]

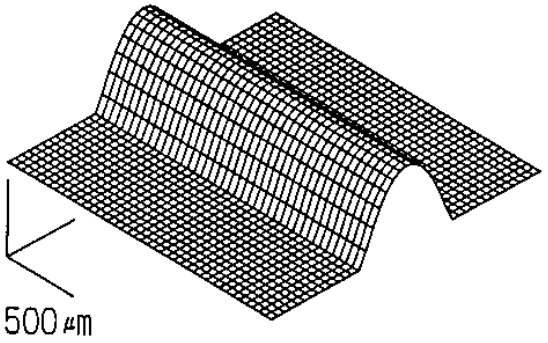

(b) Writing along a straight line [v = 50 μm/sec]

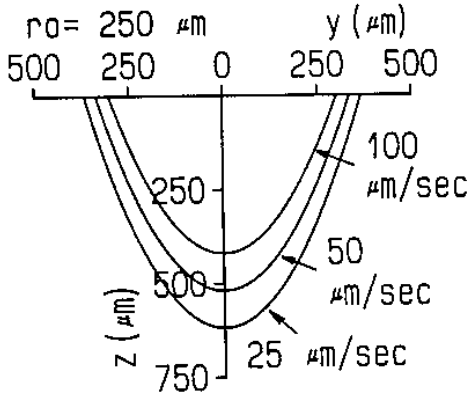

(c) Cross sectional view

Fig. 2-4 Simulation of the shape of the solidified polymer when using a gaussian beam [I_o = 1 mW/mm^2, r_o = 250 μm]

The difference, however, becomes 130 μm when a gaussian beam is used. The above analysis indicates that the solidified width with better tolerance can be obtained using a square or circular beam.

2.3.2 Comparison with experimental data

This section describes the experimental parameters and data obtained by examining the cross sections of the solidified polymer, and a comparison is made between the simulated values and experimental data.

The light source used in this experiment is a He-Cd laser (wavelength 325 nm). The laser beam is directed towards the polymer and passes through a beam expander as shown in Fig. 2-5. This produces a broad beam which facilitates the use of the central flat portion of the gaussian intensity distribution. This beam then passes through a square or circular aperture and is irradiated onto the surface of the polymer set horizontally on an X-Y table. Direct writing is then done by moving the X-Y table controlled by a computer.

Comparison of the theoretical and experimental data can be done at various intervals between the mask and polymer surface. The smaller the interval h, the smaller the difference in width of the solidified polymer. For h = 10 μm, the theoretical calculation shows a difference of several micrometers. As a tolerance of several micrometers is difficult to measure, a larger, more easily measurable difference facilitates comparison of the theoretical and experimental values. The interval between the mask and polymer surface is thus kept at several thousand micrometers.

Fig. 2-6 shows plots of optical measurements taken from cross sections of solidified polymer compared with the calculated outlines. The sidewalls of the theoretically calculated outlines match closely those of the experimental plots. The theoretically calculated outline for a square beam shows a sharp edge at the corner on the bottom of the solidified polymer. The experimental plot, however, does not have a sharp edge. This is attributed to the developer, which dissolves the bottom edge easily.

2.4 Profile simulation and experimental results

The shapes of the solidified polymer produced using beams with gaussian and uniform intensity distributions are examined along rectangular and circular profiles.

2.4.1 Rectangular profiles

In order to obtain a solidified polymer of a rectangular profile, the X-Y table moves along a straight line, stops for a time, t_s, and then moves perpendicularly in a straight line. This section examines the shape of the solidified polymer that can be obtained in this manner.

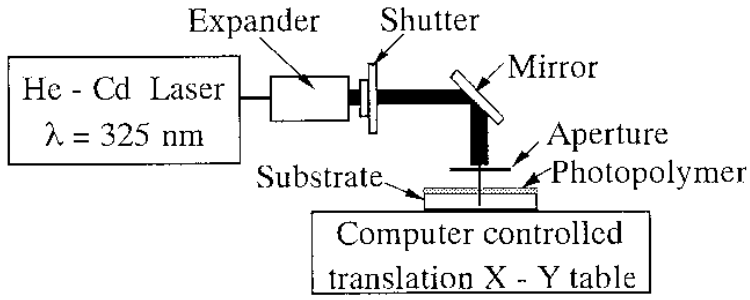

Fig. 2-5 Schematic layout of the experimental setup

The shapes of the solidified polymer at the straight line and corner portions are not the same, due to a longer irradiation time in the inner portion of the corner even when the stationary time approaches zero. This stationary time is unavoidable in using any apparatus, thus making it necessary to consider the stationary time in determining the shape of the solidified polymer. The corner shape of the solidified polymer becomes the profile (x,y,z) satisfying equation (2-4).

$$\int_0^{+\infty} [I(x-vt, y, z) + I(x, y-vt, z)]\,dt + I(x, y, z)\,t_s = E_o \tag{2-4}$$

Where I is the intensity of the light at depth z as described in equation (1-12) or (2-1).

Fig. 2-7 (a), (b) and (c) show the theoretically calculated profiles of the solidified polymer when the stationary time, t_s, is 0, 2.17 and 30 seconds, respectively. The stationary time of the apparatus used in this experiment is 2.17 seconds.

Fig. 2-8, 2-9 and 2-10 indicate the shape of the solidified polymer made using a square, circular and gaussian beams, respectively. (a) and (b) show the simulation plot and scanning electron micro graph of the experimentally obtained solidified polymer, respectively. The shapes are obtained when the stationary time is 2.17 seconds. The shapes of the simulated profiles closely resemble those obtained experimentally. There is a difference in depth between the inner and outer sides of the solidified polymer due to a longer irradiation time on the inner side. When writing with a square or circular beam, the width of the solidified polymer in the corner increases slightly while the increment when using a gaussian beam is significant. Fig. 2-11 shows the shape of the solidified polymer when writing at a high speed and long stationary time. In this case, the difference in the width of the solidified polymer between the straight line portion and the corner portion becomes large. When writing with a square or a circular beam, the difference is about 10%. When writing with a gaussian beam, however, the width in the corner is twice that of the straight line portion.

The above analysis of the simulation and experimental profiles reveal that a determined solidified polymer with a closer tolerance can be obtained using a beam of uniform intensity.

2.4.2 Circular profiles

When the radius of the arc is R and the writing speed is v, the shape of the solidified polymer becomes the (x,y,z) profile satisfying equation (2-5).

$$\frac{R}{v}\int_{-\pi}^{+\pi} I(x - R\cdot\cos u, y - R\cdot\sin u, z)\,du = E_o \tag{2-5}$$

Fig. 2-12, 2-13 and 2-14 show the shapes of the calculated profiles obtained from equation (2-5) and the corresponding scanning electron micro graphs of the solidified polymer. When using a square beam, the width of the solidified polymer varies along the arc as shown in Fig. 2-12. The difference in the width of the maximum and minimum is 200 μm. The width however, becomes constant when using a circular beam as shown in Fig. 2-13. The above analysis demonstrates that a circular beam is effective in producing patterns with circular profiles.

2.5 Products in shaped beam writing

In order to obtain high aspect ratio products, the stacking method described in Sec.1.7 is adopted. Fig. 2-15 shows the scanning micro graph of high aspect ratio structures produced by the stacking method. (a) shows the scanning micrograph of a high aspect ratio letter pattern and structure. (b) was done in order to obtain various thickness and thus produce multidimensional struc-

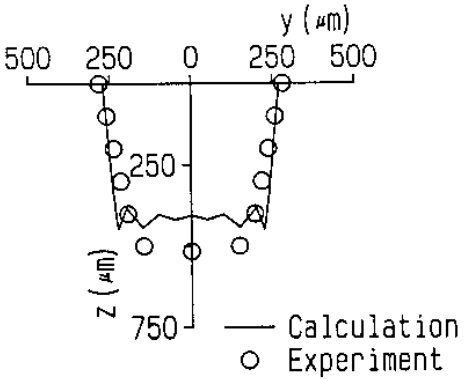

(a) A square beam [I_o = 0.53 mW/mm^2, a = 500 μm, h = 4000 μm, v = 40 μm/sec]

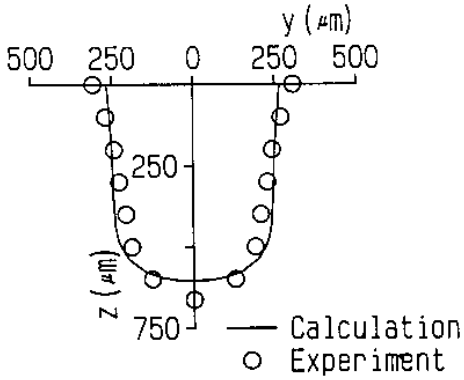

(b) A circular beam [I_o = 0.45 mW/mm^2, r_c = 250 μm, h = 2000 μm, v = 10 μm/sec]

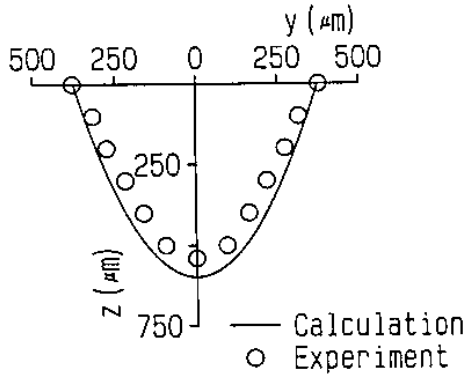

(c) A gaussian beam [I_o = 16.0 mW/mm^2, r_o = 260 μm, v = 480 μm/sec]

Fig. 2-6 Measurements from cross sections of the solidified polymer and their simulated outlines

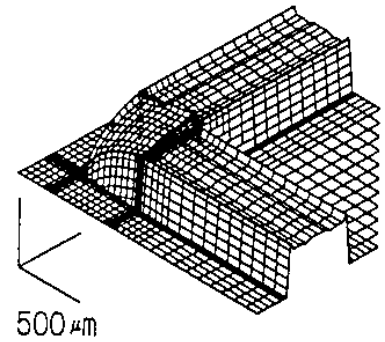

(a) t_s = 0 sec

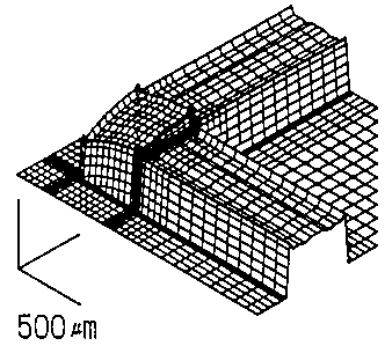

(b) t_s = 2.17 sec

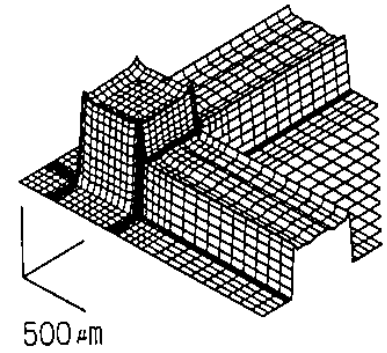

(c) t_s = 30 sec

Fig. 2-7 Simulations of the shape of the solidified polymer when writing using a square beam along a rectangular profile [I_o = 0.53 mW/mm^2, a = 500 μm, h = 2000 μm, v = 80 μm/sec]

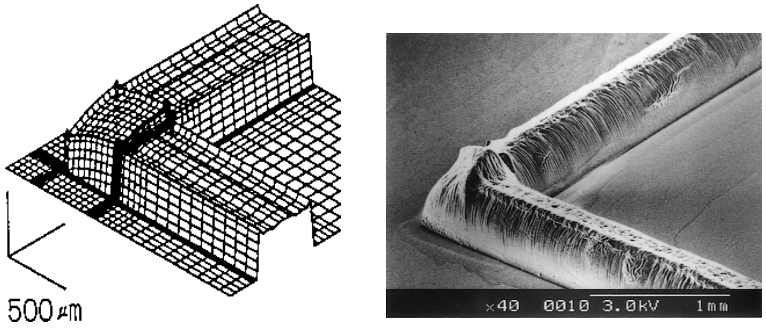

(a) Simulated profile (b) Experimental profile

Fig. 2-8 The shape of the solidified polymer when writing using a square beam along a rectangular profile [I_o = 0.53 mW/mm^2, a = 500 μm, h = 2000 μm, v = 80 μm/sec, t_s = 2.17 sec]

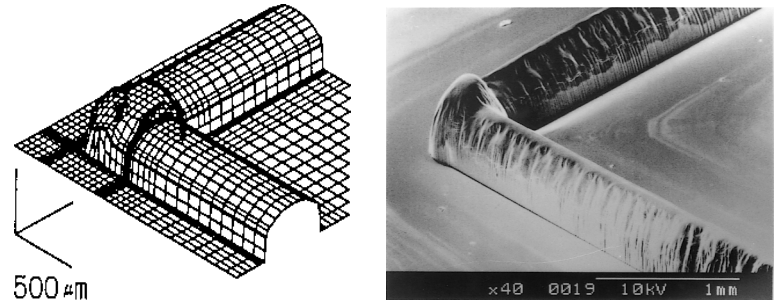

(a) Simulated profile (b) Experimental profile

Fig. 2-9 The shape of the solidified polymer when writing using a circular beam along a rectangular profile [I_o = 0.53 mW/mm^2, r_c = 250 μm, h = 2000 μm, v = 80 μm/sec, t_s = 2.17 sec]

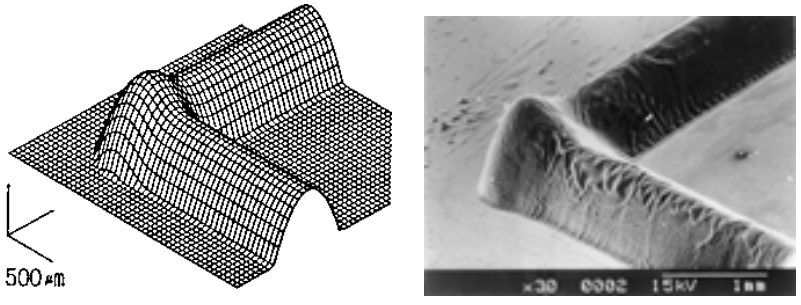

(a) Simulated profile (b) Experimental profile

Fig. 2-10 The shape of the solidified polymer when writing using a gaussian beam along a rectangular profile [I_o = 15.1 mW/mm^2, r_o = 260 μm, v = 5000 μm/sec, t_s = 2.17 sec]

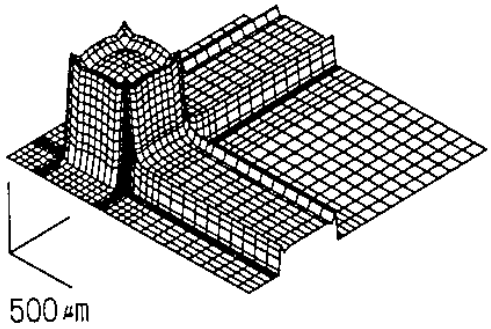

(a) A square beam [a = 500 μm, h = 2000 μm]

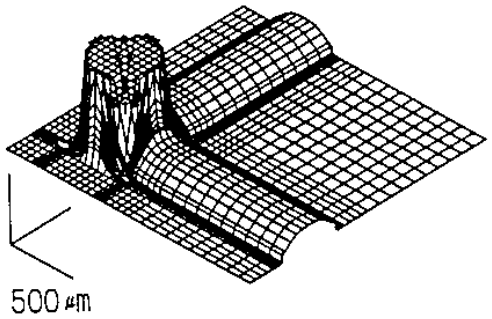

(b) A circular beam [r_c = 250 μm , h = 2000 μm]

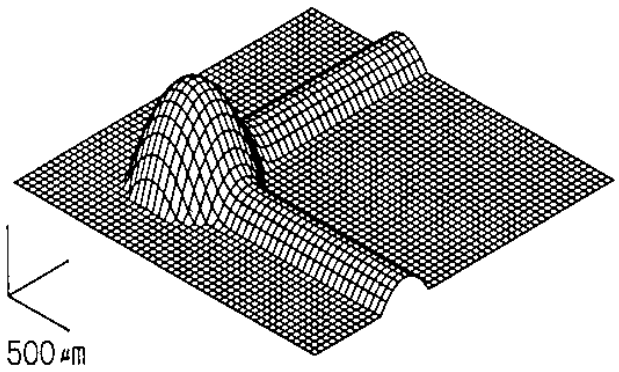

(c) A gaussian beam [r_o = 250 μm]

Fig. 2-11 Simulation of the solidified polymer when using a high writing speed and long stationary time [I_o = 1 mW/mm^2, v = 250 μm/sec, t_s = 30 sec]

tures.

Fig. 2-16 (a) shows direct writing on the surface of the polymer along the contour of a gear. (b) shows when writing on the inner side which is filled with liquid polymer. In this case, a gear structure is produced. (c) shows when writing on the outer side in which a mold is obtained.

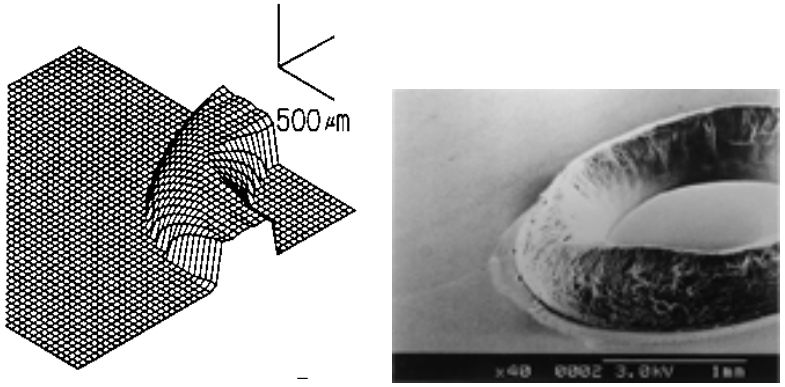

(a) Simulated profile (b) Experimental profile

Fig. 2-12 The shape of the solidified polymer when writing using a square beam along a circular profile [I_o = 0.53 mW/mm^2, a = 500 μm, h = 2000 μm, R = 1000 μm, v = 80 μm/sec]

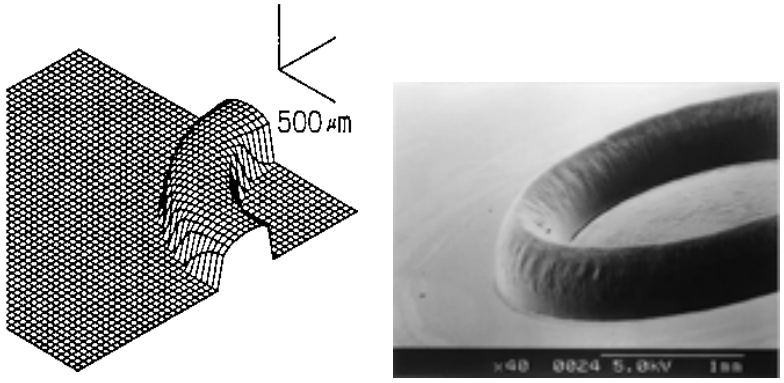

(a) Simulated profile (b) Experimental profile

Fig. 2-13 The shape of the solidified polymer when writing using a circular beam along a circular profile [I_o = 0.53 mW/mm^2, r_c = 250 μm, h = 2000 μm, R = 1000 μm, v = 80 μm/sec]

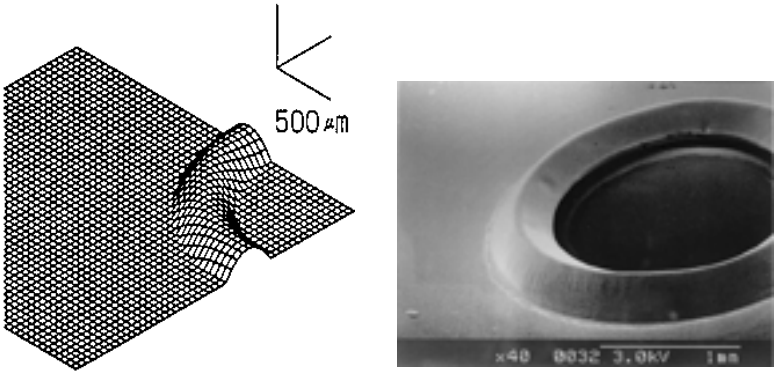

(a) Simulated profile (b) Experimental profile

Fig. 2-14 The shape of the solidified polymer when writing using a gaussian beam along a circular profile [I_o = 0.15 mW/mm^2, r_o = 260 μm, R = 1000 μm, v = 80 μm/sec]

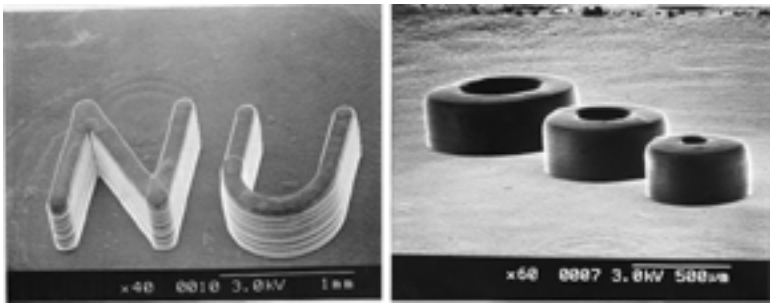

(a) High aspect ratio structures

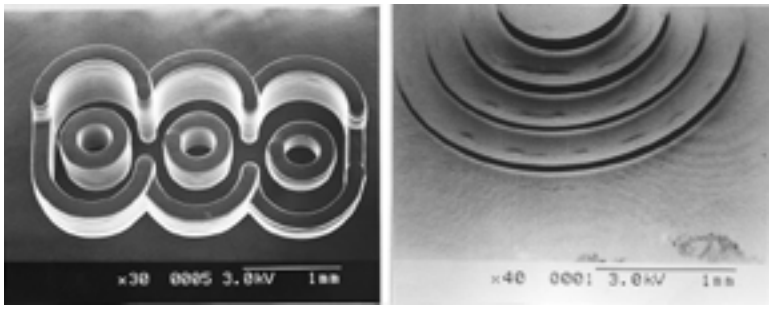

(b) High aspect ratio structures of various thickness

Fig. 2-15 Scanning micrograph of polymer structures produced by direct circular beam writing

2.6 Conclusions

The effect of writing with various shaped beams, intensity distributions, speeds and contours on the shape of the solidified polymer along the thickness when using direct writing method are examined. Based on the theoretical analysis and experimental results, the following conclusions are drawn.

(1) A solidified polymer with a close tolerance can be obtained using a beam with a uniform intensity.
(2) A circular beam is suitable in producing a pattern with combinations of various profiles.
(3) Direct laser writing can be used to produce thick, high aspect ratio microstructures by the stacking of thin polymer layers produced by overwriting.

3. Direct Focused Beam Writing Method for Producing High Aspect Ratio Micro Part

3.1 Introduction

This section examines the optimum conditions to produce high aspect ratio micro polymer structures using a direct focused UV laser beam writing on the surface of a liquid photopolymer. Various studies related to three dimensional microfabrication on polymer layers using direct writing and scanning methods have investigated the equipment and processing steps in more

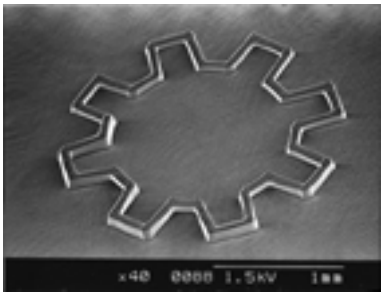

(a) Direct beam writing

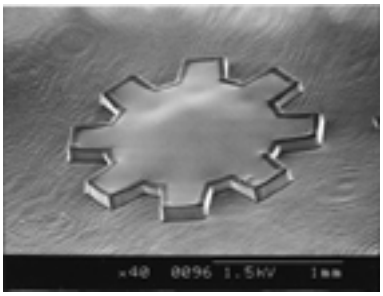

(b) Polymer structure

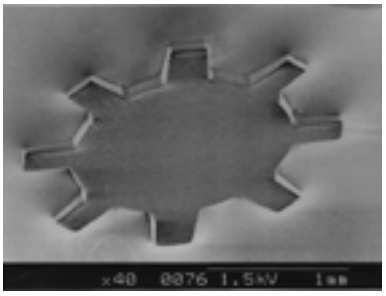

(c) Mold

Fig. 2-16 Gear structure and mold

detail[24-27,30,31,35-37]. Here the effect of physical parameters such as wavelength of laser beam, focal length of lens, absorption coefficient and writing speed on the shapes of the solidified polymer are examined theoretically. Then the results are verified experimentally. Using the theoretical and experimental results, various micropolymer structures are made with reasonably high accuracy.

3.2 Manufacturing method

The manufacture of polymer structures or molds is done by direct writing using focused UV laser beam on the surface of a liquid polymer which then becomes solid. Fig. 3-1 (a) shows a

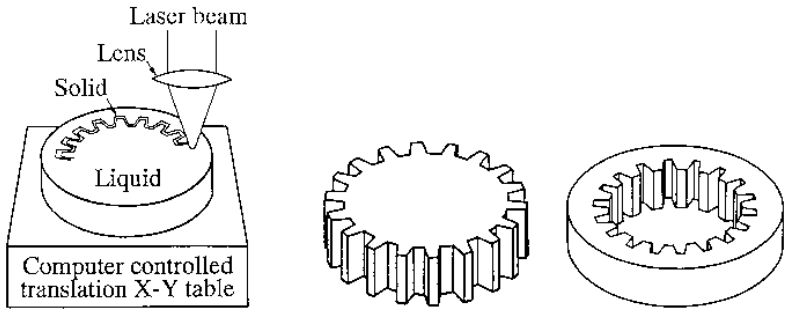

(a) Direct focused beam writing (b) Polymer structure (c) Mold

Fig. 3-1 Schematic diagram of the manufacturing method

schematic diagram of the manufacturing method used to produce micro parts with high aspect ratio. Direct laser writing along the contour produces a micro gear as shown in (b). When writing on the outer side of the contour, a mold is obtained as shown in (c). Further mold filling processes yield products of metals, plastics, and ceramics. The most common process is electroforming, in which nickel or copper material is deposited into a polymer mold.

The dimensional accuracy of the product is determined by the precision of the lateral and vertical dimensions along the thickness. The width of the solidified polymer along the thickness is affected by the shape and intensity distribution of the irradiated beam, diffraction and absorption of light within the polymer[24,28-31]. In order to produce micro polymer structures with high aspect ratio, a constant width of the solidified polymer along the depth is essential. When a beam is irradiated onto the polymer, however, the solidified width changes along the depth. Therefore it is necessary to study the solidified shape and to examine the optimum conditions to obtain a shape with a high aspect ratio.

3.3 Basic equations to shape the solidified polymer

Fig. 3-2 shows the theoretical model used to simulate the shape of the solidified polymer. Here the focal point is set at the surface of the polymer and the depth is along z. When a broad Gaussian beam with total power P, wavelength λ and radius R is irradiated passing through a lens with a focal length f, the beam intensity, I_g at (x,y,z), can be expressed as follows.

$$I_g(x, y, z) = \frac{2P}{\pi r_o^2} \cdot \exp\left[-\frac{2(x^2 + y^2)}{r_o^2}\right] \tag{3-1}$$

Here, the beam radius r_o (so-called $1/e^2$ Gaussian half-width) varies as follows.

$$r_o(z) = r_{o_{\min}} \sqrt{1 + \left(\frac{\lambda z}{\pi r_{o_{\min}}^2}\right)^2} \tag{3-2}$$

$$r_{o_{\min}} = \frac{f\lambda}{\pi R} \tag{3-3}$$

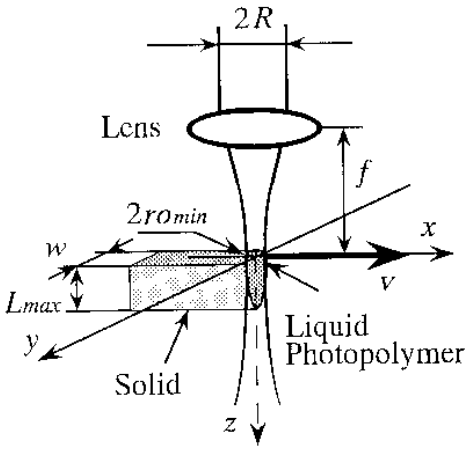

Fig. 3-2 Theoretical model

The intensity of the focused beam decreases exponentially with the beam's absorption into the polymer. Let the absorption coefficient be α. The light intensity at depth z, denoted by I, is expressed as follows.

$$I(x, y, z) = I_g(x, y, z) \cdot \exp(-\alpha z) \tag{3-4}$$

Next, the cross-sectional outline of the solidified polymer is calculated when the beam is moved along a straight line. The cross-sectional outline of the solidified polymer does not vary from point to point except for the initial point of the straight line if the writing speed is kept constant. Therefore, the cross-sectional outline of the solidified polymer is calculated when the beam is moved along the x-axis from $x = -\infty$ to $x = +\infty$ at a constant speed v as shown in Fig. 3-2. The total irradiated energy from the beam per unit area, E, at (x,y,z) can be expressed as follows.

$$E(x, y, z) = \int_{-\infty}^{+\infty} I(x - v t, y, z)\, dt \tag{3-5}$$

Here, t is the writing time. When the irradiated energy $E(x,y,z)$ attains the threshold value E_o, the polymer is assumed to solidify. By letting $E(x,y,z) = E_o$ and calculating equation (3-5), the cross-sectional outline (y,z) of the solidified polymer is expressed as equation (3-6).

$$y = \frac{r_o}{\sqrt{2}} \sqrt{\log_e\left(\sqrt{\frac{2}{\pi}} \frac{P}{E_o \cdot r_o \cdot v}\right) - \alpha z} \tag{3-6}$$

The α and E_o values of the polymer are determined experimentally. The values of the photopolymer used in this study are $\alpha = 6.94 \times 10^{-3}$ (1/μm) and $E_o = 0.34$ mJ/mm^2 as described in Sec. 1.3.

3.4 Optimum conditions to obtain high aspect ratio structures

This section examines the optimum conditions to obtain high aspect ratio micro polymer structures.

3.4.1 Physical parameters

The purpose of the theoretical analysis in this section is to examine the optimum conditions for producing high aspect ratio micro parts from equation (3-6). The outline (y,z) can be examined by considering the variables P, λ, R, f, v, E_o and α. Here, equations (3-2), (3-3) and (3-6) can be expressed as follows.

$$\frac{y}{R} = \frac{r_o/R}{\sqrt{2}} \sqrt{\log_e\left(\sqrt{\frac{2}{\pi}} \frac{P}{E_o \cdot R \cdot v} \cdot \frac{1}{r_o/R}\right) - \alpha R \frac{z}{R}} \tag{3-7}$$

$$\frac{r_o(z)}{R} = \sqrt{\frac{1}{\pi^2} \cdot \left(\frac{f}{R}\right)^2 \cdot \left(\frac{\lambda}{R}\right)^2 + \left(\frac{z/R}{f/R}\right)^2} \tag{3-8}$$

The outline $(y/R, z/R)$ of the solidified polymer is determined by λ/R, f/R, αR and $P/(E_o\, R\, v)$ corresponding to wavelength, lens, absorption and irradiation, respectively. Therefore the effects of λ, f/R and α when changing v, are examined.

3.4.2 Effect of beam wavelength λ

Fig. 3-3 (a), (b) and (c) show cross-sectional outlines of the solidified polymer when the wave length λ of the beam is 0.175 μm, 0.325 μm and 1.06 μm for the Ar-Cl laser, He-Cd laser (present experimental apparatus) and YAG laser, respectively. In these figures, the solid lines indicate the cross-sectional outlines and the broken lines the beam radius. When the writing speed is increased, the solidified depth and lateral width become smaller. When the wavelength is smaller, the solidified lateral width becomes smaller.

Next, the conditions for obtaining a high aspect ratio solidified shape are examined. In this section, only the wavelength λ is variable and other parameters such as f/R and α are constant. Fig. 3-4 shows the cross-sectional outlines of the solidified polymer when the ratio $2y(min)/2y(max)$ is maximum. Here, $2y(min)$ is the minimum solidified lateral width and $2y(max)$ is the maximum width for a depth of L = 50 μm. When the wavelength is 0.175 μm, the $2y(max)$ is 2.3 μm and the ratio $2y(min)/2y(max)$ is 0.826 as shown in Fig. 3-4 (a). When the wavelength is 1.06 μm, the ratio $2y(min)/2y(max)$ becomes 0.988; however, $2y(max)$ is 17.6 μm as shown in Fig. 3-4 (c). The solidified depth is more than 300 μm. Therefore the conditions shown in Fig. 3-4 (c) are not the optimum values to obtain high aspect ratio for a depth of 50 μm.

Fig. 3-5 (a) shows the relationship between $2y(max)$ and the wavelength. As can be seen from the figure, as the wavelength increases, $2y(max)$ increases. Fig. 3-5 (b) shows the relationship between the ratio $2y(min)/2y(max)$ and the wavelength. As the wavelength increases, the difference between $2y(min)$ and $2y(max)$ becomes minimum ($2y(min)/2y(max) \rightarrow 1$).

Here the aspect ratio of the solidified polymer is defined by the *Ratio* as follows.

$$Ratio = \frac{L}{2y(max)} \cdot \frac{2y(min)}{2y(max)} \tag{3-9}$$

For a smaller and constant solidified width, the *Ratio* for constant depth, L, becomes larger. The *Ratio* is used to find the optimum conditions. Fig. 3-6 shows the relationship between the *Ratio*

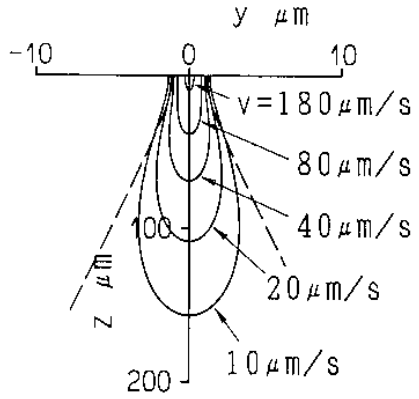

(a) λ = 0.175 μm

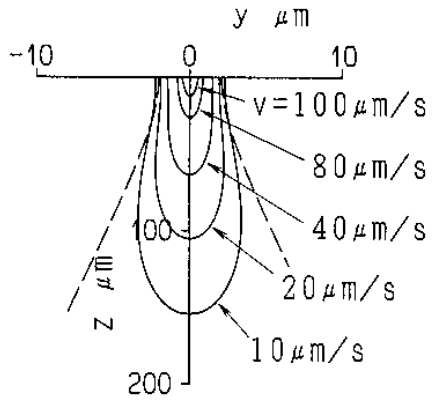

(b) λ = 0.325 μm

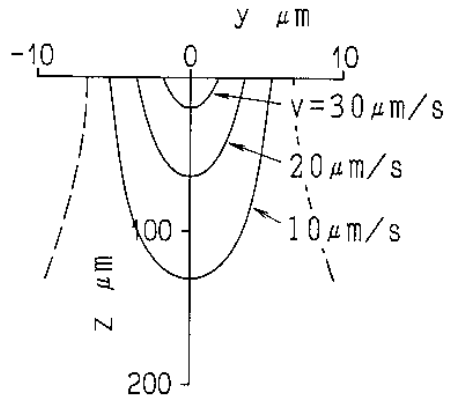

(c) λ = 1.06 μm

Fig. 3-3 Cross-sectional outlines of the solidified polymer for different wavelengths [P = 0.1 μW, f/R = 20, $\alpha = 6.94 \times 10^{-3}$ (1/μm), E_o = 0.34 mJ/mm^2]

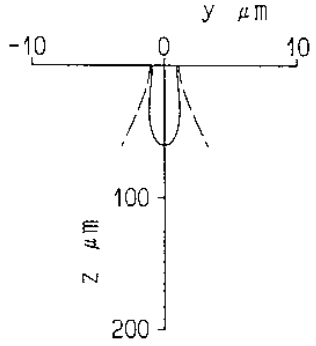

[v = 47 μm/s, 2y(*max*) = 2.3 μm, 2y(*min*)/2y(*max*) = 0.826]

(a) λ = 0.175 μm

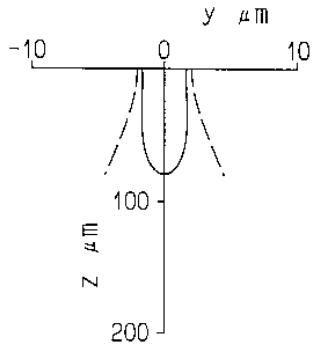

[v = 30 μm/s, 2y(*max*) = 3.5 μm, 2y(*min*)/2y(*max*) = 0.965]

(b) λ = 0.325 μm

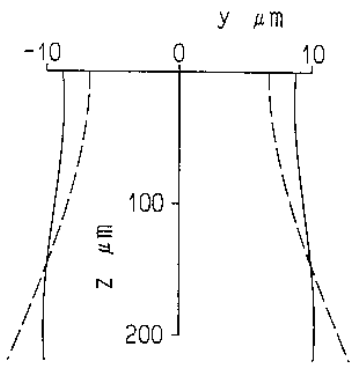

[v = 1 μm/s, 2y(*max*) = 17.6 μm, 2y(*min*)/2y(*max*) = 0.988]

(c) λ = 1.06 μm

Fig. 3-4 Cross-sectional outlines of the solidified polymer when 2y(*min*)/2y(*max*) is maximum [P = 0.1 μW, f/R = 20, $\alpha = 6.94 \times 10^{-3}$ (1/μm), E_o = 0.34 mJ/mm^2, L = 50 μm]

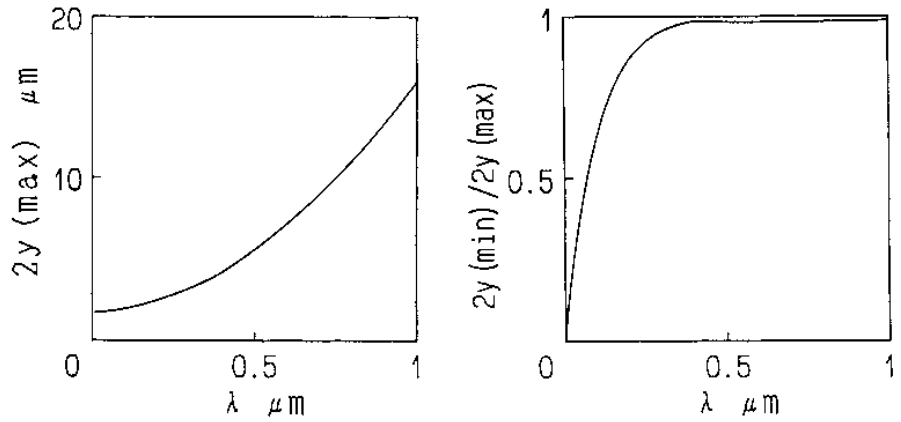

(a) 2*y*(*max*) (b) 2*y*(*min*)/2*y*(*max*)

Fig. 3-5 Relationship between 2*y*(*max*), 2*y*(*min*)/2*y*(*max*) and the wavelength [$P = 0.1\ \mu$W, $f/R = 20$, $\alpha = 6.94 \times 10^{-3}$ (1/μm), $E_o = 0.34$ mJ/mm^2, $L = 50\ \mu$m]

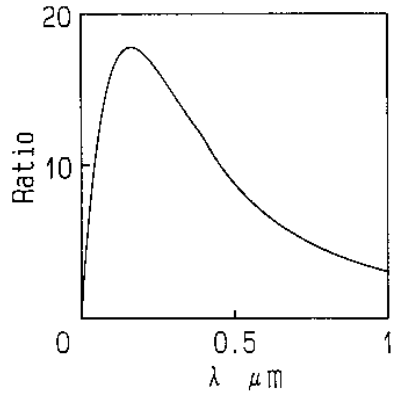

Fig. 3-6 Relationship between the *Ratio* and the wavelength [$P = 0.1\ \mu$W, $f/R = 20$, $\alpha = 6.94 \times 10^{-3}$ (1/μm), $E_o = 0.34$ mJ/mm^2, $L = 50\ \mu$m]

and the wavelength. As can be seen in this figure, the *Ratio* has the maximum value when the wavelength is 0.15 μm. Fig. 3-5 and 3-6 are examples of the optimum conditions obtained from the calculation when L is 50 μm. For other value of the L, the optimum conditions can be calculated in the same way.

3.4.3 Effect of aperture R and focal length f of lens

Fig. 3-7 shows the cross-sectional outlines of the solidified polymer when f/R is changed and other parameters are constant. When f/R is small, the minimum radius $r_{o_{min}}$ is small and the beam divergence becomes greater.

The conditions to obtain a high aspect ratio solidified shape are examined in the same way as

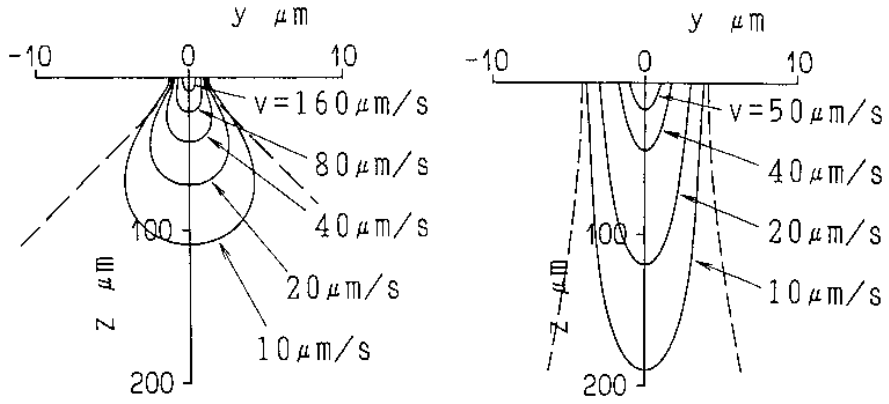

(a) $f/R = 10$ (b) $f/R = 40$

Fig. 3-7 Cross-sectional outlines of the solidified polymer for different ratios of f/R [$P = 0.1$ μW, $\lambda = 0.325$ μm, $\alpha = 6.94 \times 10^{-3}$ (1/μm), $E_o = 0.34$ mJ/mm^2]

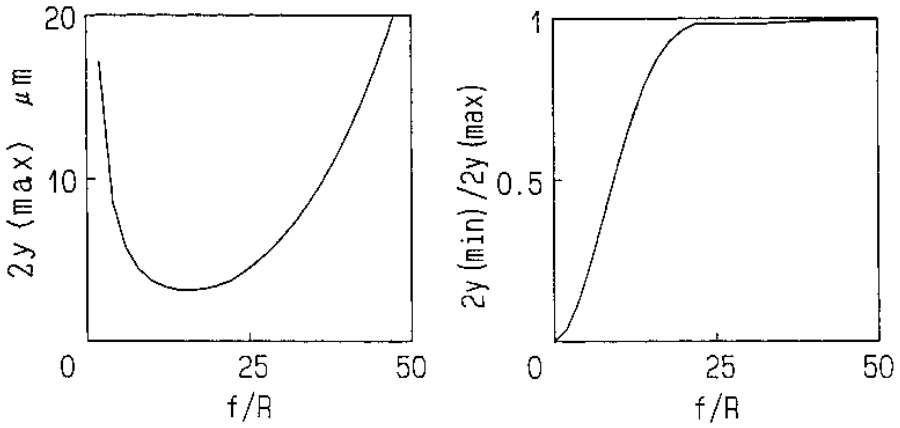

(a) $2y(max)$ (b) $2y(min)/2y(max)$

Fig. 3-8 Relationship between $2y(max)$, $2y(min)/2y(max)$ and the ratio of f/R [$P = 0.1$ μW, $\lambda = 0.325$ μm, $\alpha = 6.94 \times 10^{-3}$ (1/μm), $E_o = 0.34$ mJ/mm^2, $L = 50$ μm]

in the previous section. Fig. 3-8 (a) shows the relationship between $2y(max)$ and f/R when the ratio $2y(min)/2y(max)$ is maximum at a depth of $L = 50$ μm. When f/R is 16, the minimum value of $2y(max)$ is 3.2 μm. Fig. 3-8 (b) shows the relationship between $2y(min)/2y(max)$ and f/R. As the ratio of f/R increases, the difference between $2y(min)$ and $2y(max)$ becomes minimum ($2y(min)/2y(max) \rightarrow 1$). Fig. 3-9 shows the relationship between the *Ratio* defined in equation (3-9) and f/R. As can be seen in this figure, the *Ratio* has a maximum value when f/R is 18.

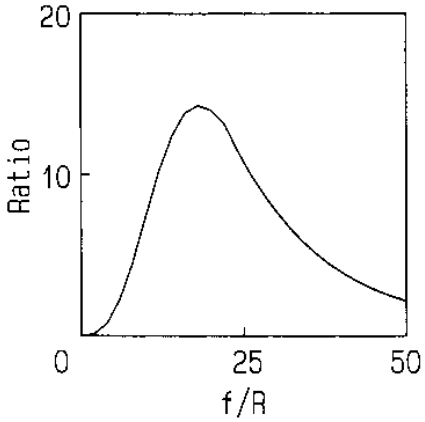

Fig. 3-9 Relationship between the *Ratio* and the ratio of *f/R* [P = 0.1 μW, λ = 0.325 μm, $\alpha = 6.94 \times 10^{-3}$ (1/μm), E_o = 0.34 mJ/mm^2, L = 50 μm]

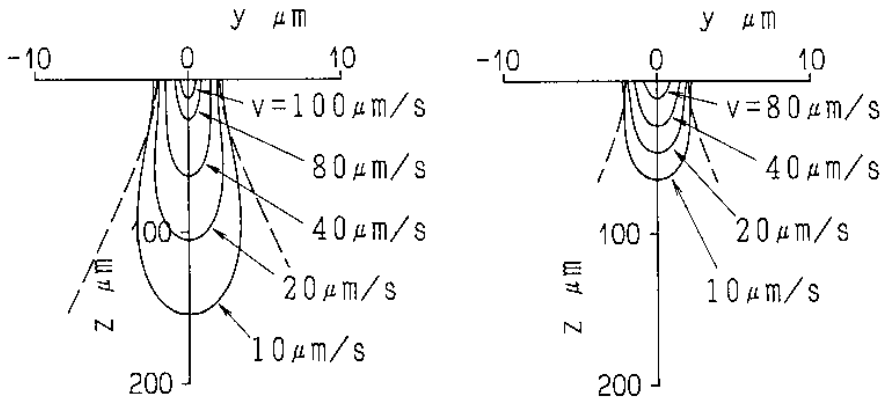

(a) $\alpha = 6.94 \times 10^{-3}$ (1/μm) (b) $\alpha = 27.76 \times 10^{-3}$ (1/μm)

Fig. 3-10 Cross-sectional outlines of the solidified polymer for different values of α [P = 0.1 μW, λ = 0.325 μm, f/R = 20, E_o = 0.34 mJ/mm^2]

3.4.4 Effect of absorption coefficient α

Fig. 3-10 shows the cross-sectional outlines of the solidified polymer when the value of α is changed and other parameters are constant. The conditions to obtain a high aspect ratio solidified shape are examined in the same way as in the previous section. Fig. 3-11 (a) shows the relationship between 2y(*max*) and α when using a condition in which the ratio 2y(*min*)/2y(*max*) becomes maximum for a depth of L = 50 μm. As the value of α increases, the 2y(*max*) increases. Fig. 3-11 (b) shows the relationship between the ratio 2y(*min*)/2y(*max*) and α. The ratio 2y(*min*)/2y(*max*) is almost constant. Fig. 3-12 shows the relationship between the *Ratio* defined in equation (3-9) and α. As can be seen in this figure, the *Ratio* becomes maximum when α is zero.

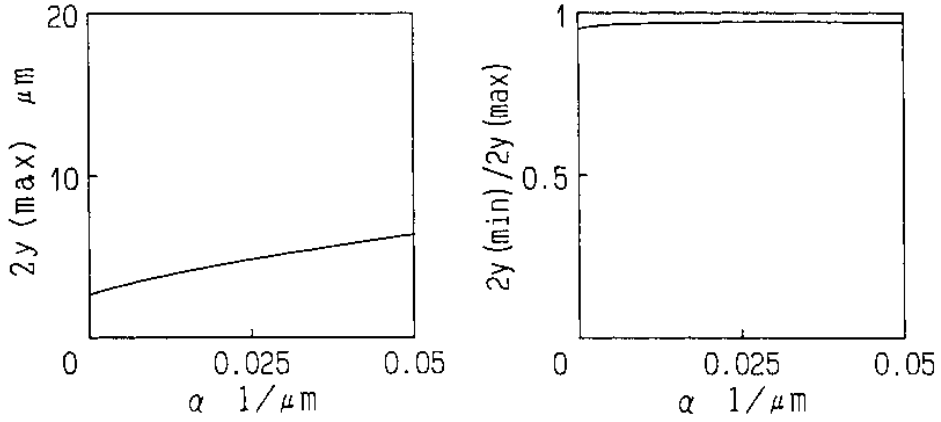

(a) 2*y*(*max*) (b) 2*y*(*min*)/2*y*(*max*)

Fig. 3-11 Relationship between 2*y*(*max*), 2*y*(*min*)/2*y*(*max*) and the value of α [P = 0.1 μW, λ = 0.325 μm, *f/R* = 20, E_o = 0.34 mJ/mm^2, L = 50 μm]

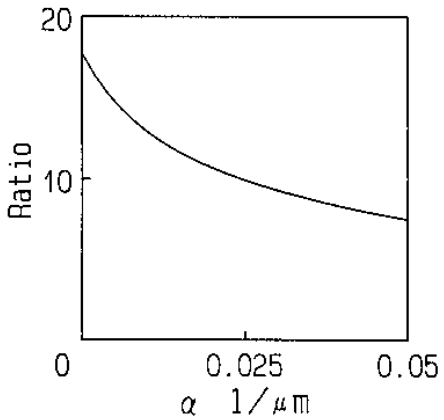

Fig. 3-12 Relationship between the *Ratio* and the value of α [P = 0.1 μW, λ = 0.325 μm, *f/R* = 20, E_o = 0.34 mJ/mm^2, L = 50 μm]

3.4.5 Effect of defocusing

The above analysis is done when the focal point is set at the surface of the polymer. Next, optimum conditions are examined when the focal point is not set at the surface of the polymer. In this analysis, the wavelength of a beam λ and the absorption coefficient α are given, and the ratio of *f/R* is determined at first.

The beam radius r_o changes according to equations (3-2), (3-3). When z is far greater than $\lambda f^2/R^2$, r_o varies as follows.

$$r_o(z) = \frac{R}{f} z \tag{3-10}$$

When the focal point is not set at the surface of the polymer, the beam radius r_o is expressed as follows.

$$r_o(z) = r_s \pm \frac{R}{f} z \tag{3-11}$$

Here, r_s is the beam radius at the surface of the polymer. When the sign in equation (3-11) is plus, the beam radius increases along the depth direction and when the sign is minus, the beam radius decreases. Here, the plus and minus signs are related to the position of the focal point when it is above and below the surface of the polymer, respectively. In this section, the calculation to obtain optimum conditions for a high aspect ratio solidified shape is approximated by equation (3-11).

The following conditions are considered to obtain the perpendicular cross-sectional outline of the solidified polymer at the surface of the polymer. These conditions can be realized only when the focal point is not set at the surface of the polymer.

$$[y]_{z=0} > 0, \qquad \left[\frac{dy}{dz}\right]_{z=0} = 0, \qquad \left[\frac{d^2y}{dz^2}\right]_{z=0} = 0 \tag{3-12}$$

Substituting equation (3-11) into equation (3-6) and differentiating as in equation (3-12) gives the following.

$$r_o(z) = r_s - \frac{3}{2}\alpha \cdot r_s \cdot z \tag{3-13}$$

$$\log_e\left(\sqrt{\frac{2}{\pi}}\frac{P}{E_o \cdot r_s \cdot v}\right) = \frac{1}{6} \tag{3-14}$$

From equation (3-13), the beam radius has a minimum value when the focal point is below the surface of the polymer. From equation (3-3), (3-11) and (3-13), the relationship between the ratio of *f*/*R*, the minimum beam radius $r_{o_{min}}$ and the beam radius at the surface r_s is expressed as follows.

$$r_s = \frac{2R}{3\alpha \cdot f} = \frac{2\lambda}{3\pi \cdot \alpha \cdot r_{o_{\min}}} \tag{3-15}$$

When the focal point is set below the surface of the polymer, the beam radius r_o is expressed exactly as follows.

$$r_o(z) = r_{o_{\min}} \sqrt{1 + \left\{\frac{\lambda (z - z_o)}{\pi r_{o_{\min}}^2}\right\}^2} \tag{3-16}$$

Here, z_o is the depth of the focal point from the polymer surface. Setting $r_o = r_s$ when $z = 0$, z_o is obtained from equation (3-16) as follows.

$$z_o = \frac{\pi \cdot r_{o_{\min}}}{\lambda} \sqrt{r_s^2 - r_{o_{\min}}^2} \tag{3-17}$$

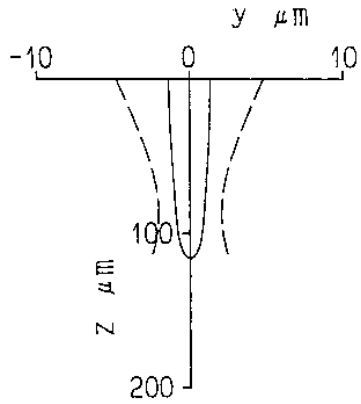

(a) When defocusing [z_o = 87 μm, v = 41 μm/sec]

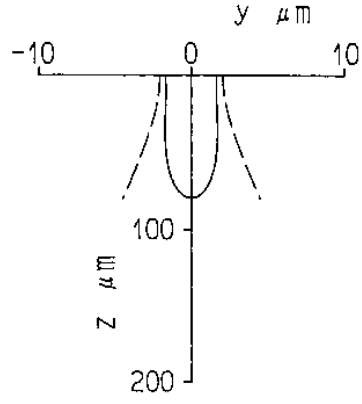

(b) When the focal point is set at the polymer surface [z_o = 0 μm, v = 30 μm/sec]

Fig. 3-13 Cross-sectional outlines of the solidified polymer [P = 0.1 μW, λ = 0.325 μm, f/R = 20, α = 6.94 × 10^{-3} (1/μm), E_o = 0.34 mJ/mm^2]

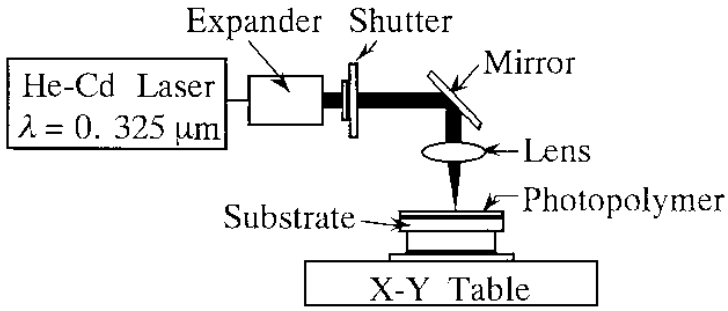

Fig. 3-14 Experimental setup

When the solidified shape is obtained according to this condition, at first the f/R is determined and the minimum beam radius $r_{o_{min}}$ is calculated using equation (3-3). Next, r_s and z_o are calculated using equations (3-15) and (3-17). At last the value P/v is calculated using equation (3-14). One value of either P or v can be chosen arbitrarily. Fig. 3-13 (a) shows an example of the cross-sectional outline of the solidified polymer under these conditions. Fig. 3-13 (b) shows the cross-sectional outline of the solidified polymer when the focal point is set at the surface of the polymer. The outline obtained in (a) shows a smaller solidified width and a higher aspect ratio compared to that shown in (b).

3.5 Comparison with experimental data

This section describes the experimental parameters and data obtained by examining the cross sections of the solidified polymer, and a comparison is made between the simulated values and experimental data.

The light source used in this experiment is a He-Cd laser (wavelength λ = 0.325 μm). The laser beam passes through a beam expander as shown in Fig. 3-14. The radius of the beam before

entering the lens, *R*, is about 3.6 mm. This broad beam is then focused by a lens and is irradiated onto the surface of the polymer set horizontally on an X-Y table. In this experiment, the focal point is set at the surface of the polymer and direct writing is done by moving the X-Y table controlled by a computer. The photopolymer used in this experiment is a product of Asahi Chemical Co., Ltd.

Fig. 3-15 (a), (b) and (c) show plots of measurements of cross sections of the solidified polymer compared with the calculated outlines. The theoretically calculated outlines match closely those of the experimental plots. In figure (a), the solidified width is 10 μm. The accuracy of the solidified width measured at the surface and at a depth of 100 μm is 0.5μm. The accuracy of the solidified width measured at the surface and at a depth of 200 μm is 2 μm. The aspect ratios when obtaining an accuracy of 0.5 μm and 2 μm are 10 and 20, respectively.

3.6 Examples of high aspect ratio products

Using the above results, the high aspect ratio solidified shapes can be produced as shown in Fig. 3-16. (a) shows a polymer structure of a micro pump. (b) shows a micro gear and a human hair is set alongside by way of comparison. (c) shows a cell vessel used for use in biotechnology and (d) a letter pattern. Fig. 3-17 gives an example of a piled-up structures.

3.7 Conclusions

(1) The effects of wavelength of beam, focal length of lens, absorption coefficient of the polymer and writing speed are examined when using direct focused beam writing. The optimum conditions to obtain a high aspect ratio polymer shapes are examined.
(2) Using the above conditions, high aspect ratio micro mechanical structures are produced.

4. Manufacturing of Three-Dimensional Structures

4.1 Introduction

This section deals with the manufacturing of three-dimensional micro polymer structures. At first, the optimum conditions to produce the stacked three-dimensional structures are verified. Next, by using these conditions, stacked three-dimensional structures are produced.

4.2 Manufacturing method

Fig. 4-1 shows a schematic diagram of the manufacturing method to produce three-dimensional micro-polymer structures by stacking the polymer layers on top of one another.

4.3 Conditions for producing three-dimensional microstructures

When stacked three-dimensional microstructures are produced, a large value of the solidified depth becomes the error in the vertical direction. And the solidified depth is chosen near the value of the solidified width for the direct writing method. On this condition, a small depth of the solidified polymer is essential, and the solidified depth is smaller than the depth of focus of the beam. Therefore the beam can be approximated using the parallel beam with the radius $r_{o_{min}}$. From equation (3-6), the maximum solidified depth, L_{max}, and the solidified width, *w*, at the surface of the photopolymer are expressed as follows.

$$L_{\max} = \frac{1}{\alpha} \log_e \left(\sqrt{\frac{2}{\pi}} \cdot p_n \right) \tag{4-1}$$

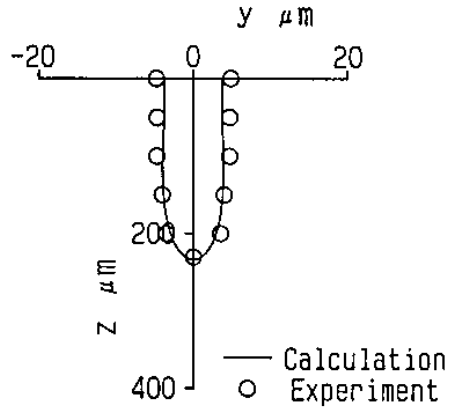

(a) v = 10 μm/sec

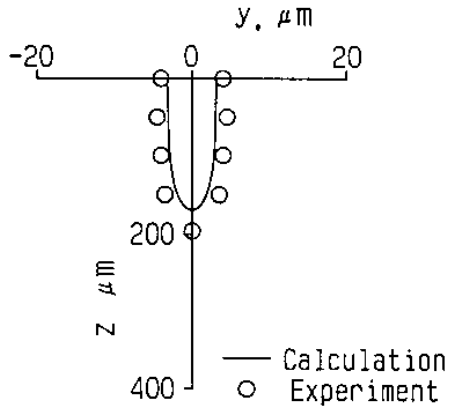

(b) v = 20 μm/sec

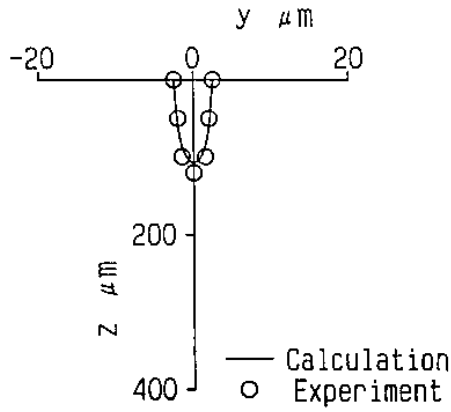

(c) v = 40 μm/sec

Fig. 3-15 Cross section of the solidified polymer (With focal point set at the polymer surface) [P = 0.17 μW, λ = 0.325 μm, R = 3.62 mm, f = 120 mm, $\alpha = 6.94 \times 10^{-3}$ (1/μm), E_o = 0.34 mJ/mm^2]

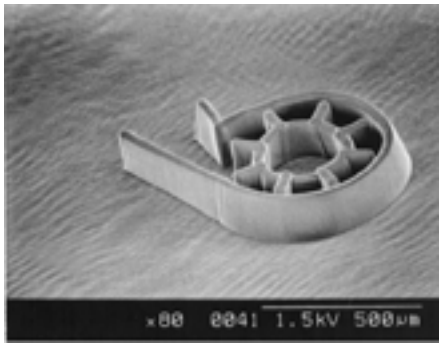

(a) Micro pump

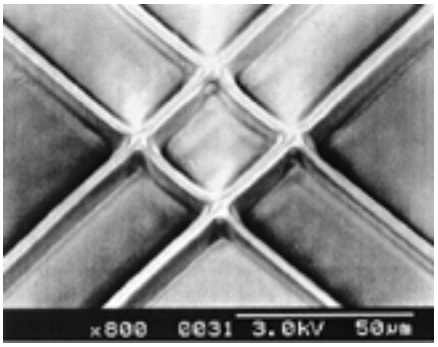

(c) Micro cell

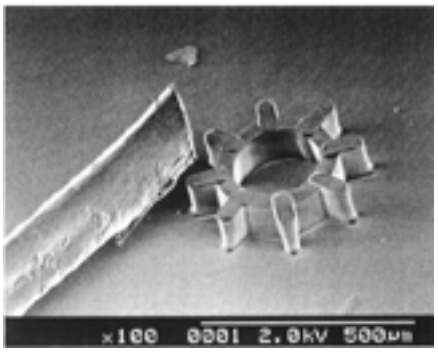

(b) Micro gear

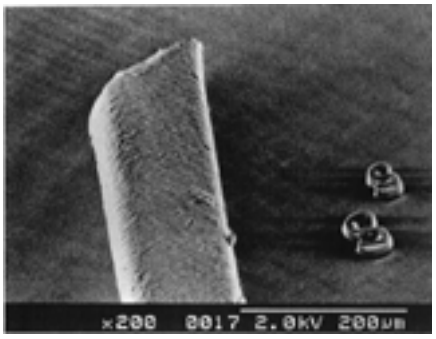

(d) Letter pattern

Fig. 3-16 Example of polymer structures produced by direct focused beam writing

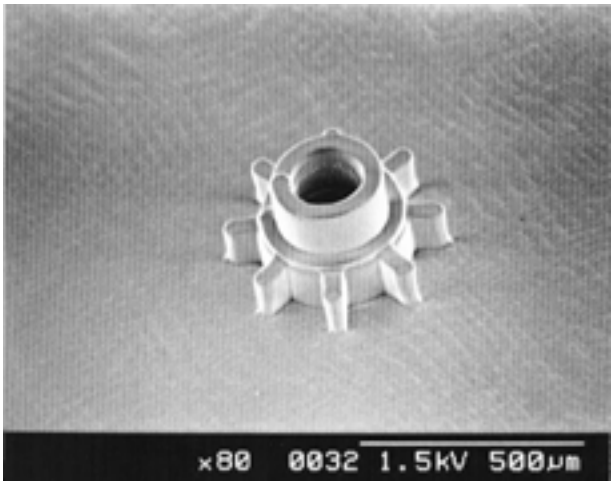

Fig. 3-17 An example of a piled-up structure

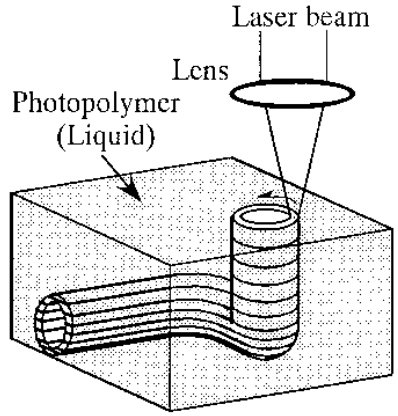

Fig. 4-1 Schematic diagram of the manufacturing method for a three-dimensional microstructure

$$w = \sqrt{2}\, r_{o\min} \sqrt{\log_e\left(\sqrt{\frac{2}{\pi}} \cdot p_n\right)} \tag{4-2}$$

Here, p_n is a non-dimensional value corresponding to the irradiation of the beam and is expressed as follows.

$$p_n = \frac{P}{E_o \cdot r_{o\min} \cdot v} \tag{4-3}$$

From equation (4-1), the maximum solidified depth is determined by the value of irradiation p_n and the absorption coefficient α. Fig. 4-2 (a) shows the cross-sectional outlines for different vales of α. When the value of α is small, the maximum solidified depth attains over 100 μm and the depth is not suitable to produce micro parts. By increasing the value of α, the solidified depth can be decreased. For example, when α is 4.9×10^{-2} (1/μm), the solidified depth is almost the same as the solidified depth. Fig. 4-2 (b) shows the cross-sectional outlines for different values of p_n. By changing the value of p_n, the solidified depth can be changed. However, the solidified width is also changed. From Fig. 4-2 (a) and (b), the solidified depth can be changed by varying the value of α or p_n. Therefore there are numerous combinations between the α and p_n in order to obtain the desired solidified depth.

Next, the optimum combinations between the α and p_n are verified. When writing along a contour with corners or stationary points, the value of the irradiation is varied. Therefore, it is necessary to consider the conditions to obtain the constant solidified depth in this case. From equation (4-1), when the value of p_n is changed by Δp_n, the fluctuation of L_{max} is expressed as follows.

$$\Delta L_{\max} = \frac{1}{\alpha} \cdot \frac{\Delta p_n}{p_n} \tag{4-4}$$

Fig. 4-3 shows cross-sectional outlines of the solidified polymer for different values of the absorption coefficient α, when $\Delta p_n/p_n$ is ±10%. From Fig. 4-3 and equation (4-4), the larger absorption

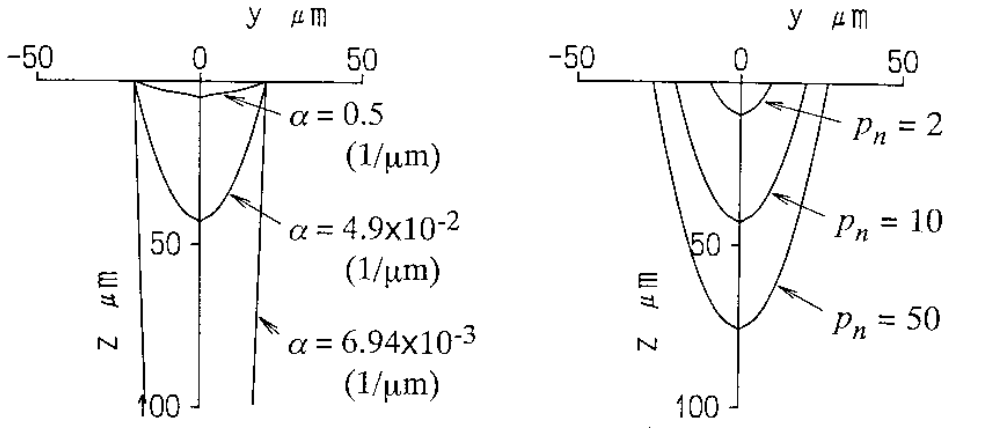

(a) Different values of α [$p_n = 10$] (b) Different values of p_n [$\alpha = 4.9 \times 10^{-2}$ (1/μm)]

Fig. 4-2 Cross-sectional outlines of the solidified polymer [$\lambda = 0.325$ μm, $f/R = 192$, $v = 10$ μm/sec, $E_o = 0.34$ mJ/mm^2]

coefficient becomes, the smaller is the fluctuation ΔL_{max}. However, the solidified width at the surface w becomes large when the absorption coefficient is too large.

The optimum condition can be calculated from equations (4-1)-(4-4) in order to obtain the desired maximum solidified depth and solidified width with reasonable fluctuation. The procedure is as follows. At first, the maximum solidified depth L_{max} and solidified width w are given. The absorption coefficient α can be calculated from equation (4-4) by the degree of fluctuation. Next $r_{o_{min}}$ and p_n are calculated from equation (4-1) and (4-2). For example, $\alpha = 5 \times 10^{-2}$ (1/μm), $r_{o_{min}} = 20$ μm and $p_n = 9.3$ are obtained when the $L_{max} = 40$ μm, $w = 40$ μm and $\Delta L_{max} = 2$ μm ($\Delta p_n / p_n = \pm 10\%$).

4.4 Rectangular profile

The effect of the above analysis is shown by the rectangular profile. When writing along a rectangular profile, the solidified shape is expressed as follows.

$$z = \frac{1}{\alpha} \log_e \left\{ \frac{\sqrt{2}P}{\pi \cdot r_{o\min} \cdot E_o \cdot v} \times \left[\left(\int_0^{\frac{\sqrt{2}x}{r_{o\min}}} \exp\left(-q^2\right) dq + \frac{\sqrt{\pi}}{2} \right) \cdot \exp\left(-\frac{2y^2}{r_{o\min}^2} \right) + \left(\int_0^{\frac{\sqrt{2}y}{r_{o\min}}} \exp\left(-q^2\right) dq + \frac{\sqrt{\pi}}{2} \right) \cdot \exp\left(-\frac{2x^2}{r_{o\min}^2} \right) \right] \right.$$

$$+\frac{2P\cdot t_s}{\pi\cdot r_{o\min}^2\cdot E_o}\cdot\exp\left(-\frac{2(x^2+y^2)}{r_{o\min}^2}\right)\Bigg\} \tag{4-5}$$

In equation (4-5), t_s is the stationary time at the corner. Fig. 4-4 shows the theoretically calculated profile. When the absorption coefficient is small, the difference in the solidified depth between the straight portion and the corner portion is large. The difference becomes small, and it becomes easy to obtain the constant value of the solidified depth by choosing the absorption coefficient according to the analysis provided in the previous section.

4.5 Comparison with experimental data

The absorption coefficient of the photopolymer used in this experiment is 6.94×10^{-3} ($1/\mu$m), a value too small to obtain a constant solidified depth. Therefore, by the addition of Rhodamine B ($C_{28}H_{31}ClN_2O_3$), the value of the absorption coefficient is increased and the value chosen is 4.9×10^{-2} ($1/\mu$m) from the analysis of the previous section.

Fig. 4-5 shows the plots of optical measurements of the cross sections of the solidified polymer compared with the calculated outlines. The theoretically calculated outlines match those of the experimental plots. The difference in the width or depth between the calculation and experiment is $\pm5\,\mu$m.

4.6 Stacked structure

Three-dimensional solidified polymer structures are attained by stacking two-dimensional polymer structures, and the stacked profile is examined. For example, Fig. 4-6 shows the schematic diagram of the cross section of a wall structure with an angle of 60 degrees. The waviness of the left side *WL* and the right side *WR* are expressed as follows.

$$WL=\frac{h^2\cdot\cos^2\theta}{2\alpha\cdot r_{o\min}^2\cdot\sin^3\theta} \tag{4-6}$$

$$WR=\frac{r_{o\min}\cdot\sin\theta}{\sqrt{2}}\left[\sqrt{\log_e\left(\sqrt{\frac{2}{\pi}}\,\frac{P}{E_o\cdot r_{o\min}\cdot v}\right)}-\sqrt{\log_e\left(\sqrt{\frac{2}{\pi}}\,\frac{P}{E_o\cdot r_{o\min}\cdot v}\right)-\alpha\cdot h}\right]+h\cdot\cos\theta \tag{4-7}$$

In equations (4-6) and (4-7), h is the interval of each stacked polymer layer.

Fig. 4-6 (b) is a scanning micrograph of the stacked structure. The micrograph has a profile similar to that of the calculated profile. When *h* becomes 10 μm, the wall has the surface waviness of 1 μm and 7 μm on each side.

From the above results, the accuracy of 5 μm in the width or depth and the waviness of 1 μm in the side wall can be attained. Fig. 4-7 provides examples of three-dimensional micro polymer structures. (a) shows the micro pipe illustrated as Fig. 4-1; (b) is a micro ball and (c) is a micro cup. The crossed ring (d) can be also produced.

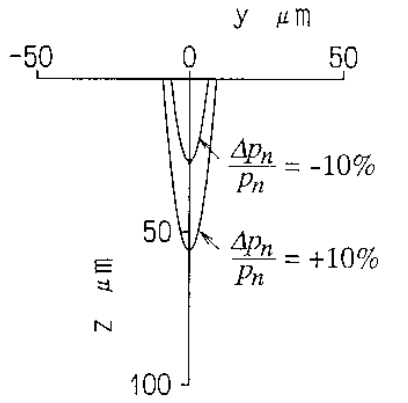

(a) $\alpha = 6.94 \times 10^{-3}$ (1/μm) [$P = 0.114\ \mu$W]

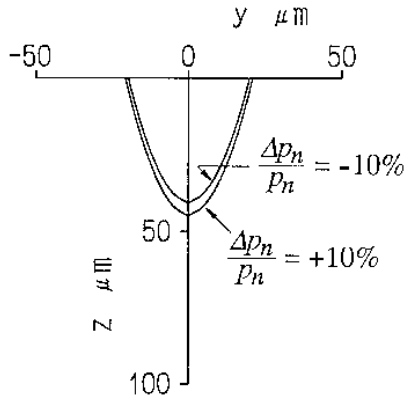

(b) $\alpha = 4.9 \times 10^{-2}$ (1/μm) [$P = 0.676\ \mu$W]

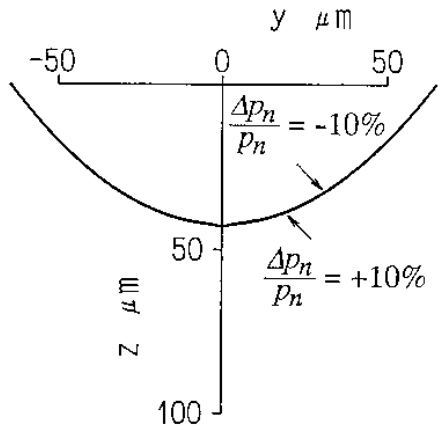

(c) $\alpha = 0.5$ (1/μm) [$P = 135$ W]

Fig. 4-3 Fluctuation of the solidified depth with the fluctuation of irradiation [$\Delta p_n / p_n = \pm 10\%$, $\lambda = 0.325\ \mu$m, $f/R = 192$, $v = 10\ \mu$m/sec, $E_o = 0.34$ mJ/mm^2]

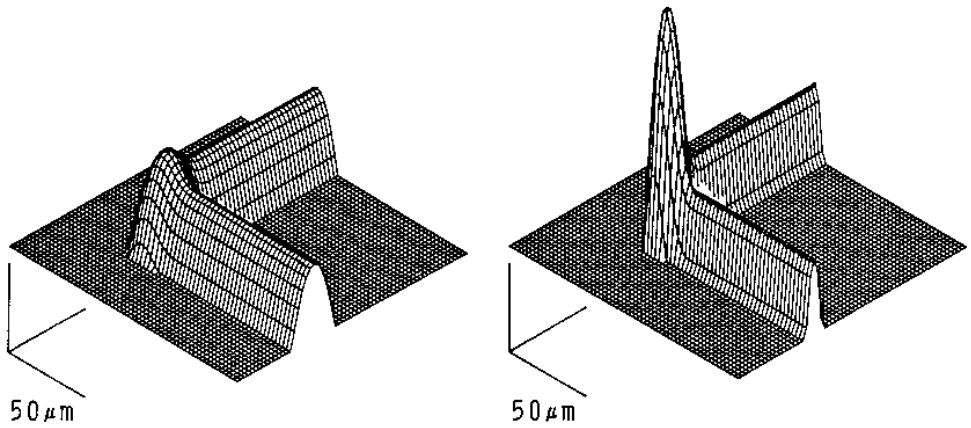

(a) $\alpha = 5 \times 10^{-2}$ (1/μm) [$P = 0.676$ μW] (b) $\alpha = 6.94 \times 10^{-3}$ (1/μm) [$P = 0.114$ μW]

Fig. 4-4 Solidified shape when writing along a rectangular profile [$\lambda = 0.325$ μm, $f/R = 192$, $v = 10$ μm/sec, $t_s = 2.17$ sec, $E_o = 0.34$ mJ/mm^2]

4.7 Conclusions

(1) The effects of beam wavelength, focal length of lens, absorption coefficient of the polymer and writing speed on the shape of the solidified polymer are examined when using direct focused beam writing on the surface of a photopolymer.
(2) The optimum conditions to obtain high aspect ratio polymer structures and stacked three-dimensional structures are verified.
(3) Using the above conditions, microstructures are produced.

Acknowledgement

The present work was supported by a Grant-in-Aid for Scientific Research (B) No. 10555038 from the Ministry of Education, Science, Sports and Culture, Japan.

References

1) Mehregany, M., Gabriel, K. J. and Trimmer, W. S. N., Integrated Fabrication of Polysilicon Mechanisms, IEEE Trans. Electron Devices, Vol.35, No.6 (1988), pp. 719–723.
2) Fan, L. S., Tai, Y. C. and Muller, R. S., Integrated Movable Micromechanical Structures for Sensors and Actuators, IEEE Trans. Electron Devices, Vol.35, No.6 (1988), pp. 724–730.
3) Fan, L. S., Tai, Y. C. and Muller, R. S., IC-Processed Electrostatic Micromotors, Proc. of the 1988 IEEE Electron Devices Meeting, San Francisco, CA, Dec. 11-14 (1988), pp.666–669.
4) Roylence, L. M. and Angell, J. B., A Batch-Fabricated Silicon Accelerometer, IEEE Trans. on Electron Devices, Vol. ED-26, No. 12 (1979), pp. 1911–1917.
5) Petersen, K. E., Shartel, A. and Raley, N. F., Micromechanical Accelerometer Integrated with MOS Detection Circuitry, IEEE Trans. on Electron Devices, Vol. ED-29, No. 1 (1982), pp. 23–27.

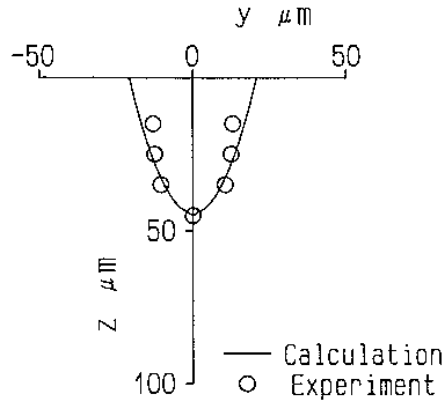

(a) $P = 0.74\,\mu$W

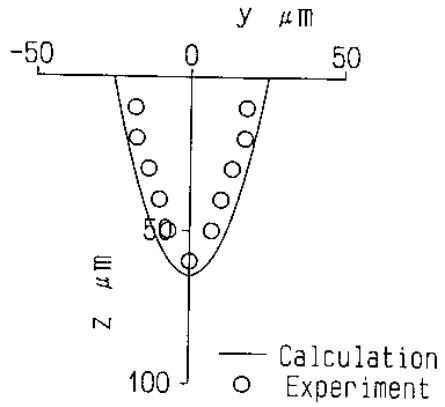

(b) $P = 2.0\,\mu$W

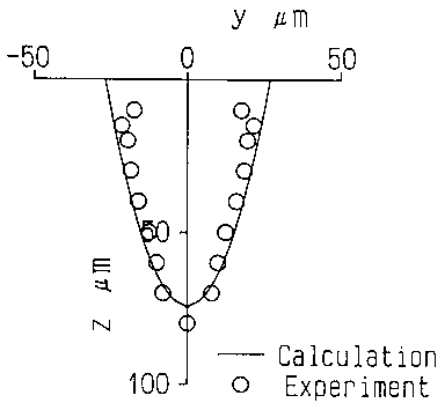

(c) $P = 3.2\,\mu$W

Fig. 4-5 Experimental plots of the cross section of the solidified polymer (With focal point set at polymer surface) [$\lambda = 0.325\,\mu$m, $f/R = 192$, $v = 10\,\mu$m/sec, $\alpha = 4.9 \times 10^{-2}$ (1/μm), $E_o = 0.34$ mJ/mm^2]

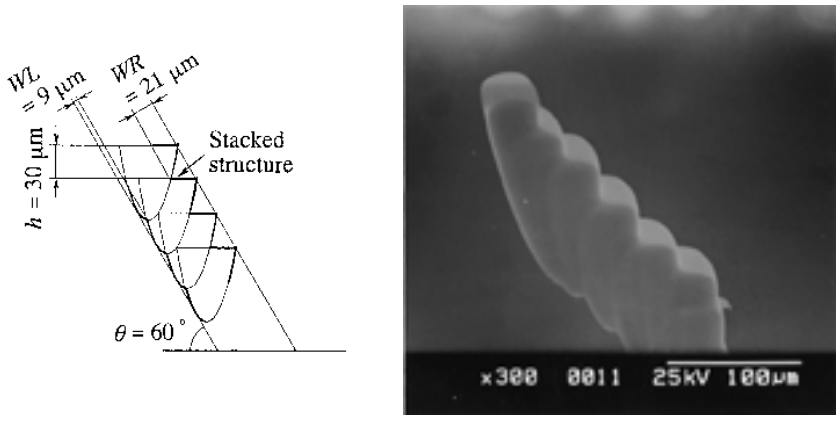

(a) Calculated profile (b) Micrograph

Fig. 4-6 Stacked profile [P = 2.0 μW, λ = 0.325 μm, f/R = 192, v = 10 μm/sec, α = 4.9 × 10^{-2} (1/μm), E_o = 0.34 mJ/mm^2, θ = 60 deg., h = 30 μm]

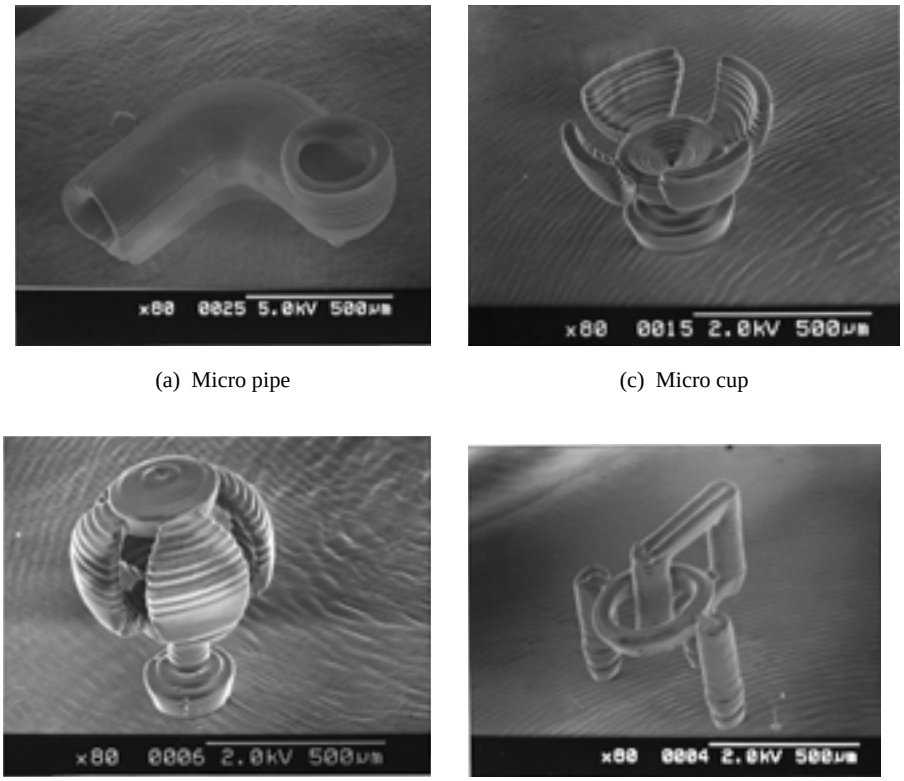

(a) Micro pipe (c) Micro cup

(b) Micro ball (d) Micro ring

Fig. 4-7 Example of three-dimensional polymer structures produced by direct focused beam writing

6) Ehrfeld, W., The LIGA Processes for Microsystems, Micro System Technologies 90, Proceedings of 1st International Conference on Micro Electro, Opto, Mechanic Systems and Components, Berlin, (1990), pp. 521–528.
7) Mohr, J., Burbaum, C., Bley, P., Menz, W. and Wallrabe, U., Movable Microstructures Manufactured by the LIGA Process as Basic Elements for Microsystems, MicroSystem Technologies 90, Proc of 1st Int. Conf. on Micro Electro, Opto, Mechanic Systems and Components, Berlin (1990), pp. 529–537.
8) Menz, W., Bacher, W., Harmening, M. and Michel, A., The LIGA Technique — a Novel Concept for Microstructures and the Combination with Si-Technologies by Injection Molding, Proceedings of IEEE Micro Mechanical Systems, Japan, Nara (1991), pp. 69–73.
9) Menz, W., Microactuators in LIGA Technique, Int. Journal of Applied Electromagnetics in Materials, Vol. 2, No. 4 (1992), pp. 281–284.
10) Mohr, J., Anderer, B. and Ehrfeld, W., Fabrication of a Planar Grating Spectrograph by Deep-etch Lithography with Synchrotron Radiation, Sensors and Actuators, A: Physical, Vol. 27, No. 1–3 (1991), pp. 571–575.
11) Maner, A. and Ehrfeld, W., Electroforming Technique in the LIGA Process for the Production of Microdevices, Materials and Manufacturing Process, Vol. 4, No. 4 (1989), pp. 527–537.
12) Becker, E. W., Development of the Separation Nozzle Process for Enrichment of Uranium, German Chemical Engineering, Vol. 9, No. 4 (1986), pp. 204–208.
13) Becker, E. W., Ehrfeld, W., Hagmann, P., Maner, A. and Muenchmeyer, D., Fabrication of Microstructures with High Aspect Ratio and Great Structural Height by Synchrotron Radiation Lithography, Microelectronic Engineering, Vol. 4, No. 1 (1986), pp. 35–56.
14) Rogner, A., Ehrfeld, W., Muenchmeyer, D., Bley, P., Burbaum, C. and Mohr, J., LIGA Based Flexible Microstructures for Fiber-chip Coupling, Journal of Micromechanics and Microengineering, Vol. 1, No. 3 (1991), pp. 167–170.
15) Guckel, H., Skrobis, K. J., Christenson, T. R., Klien, J., Han, S., Choi, B., Lovell, E. G. and Chapman, T. W., Fabrication and Testing of the Planar Magnetic Micromotor, Journal of Micromechanics and Microeng., Vol. 1, No. 3 (1991), pp. 135–138.
16) Burbaum, C., Mohr, J., Bley, P. and Ehrfeld, W., Fabrication of Capacitive Acceleration Sensors by LIGA Technique, Sensors and Actuators, A: Physical, Vol. 27, No. 1-3 (1991), pp. 559–563.
17) Guckel, H., Christenson, T., Skrobis, K., Metal Micromechanisms via Deep X-ray Lithography, Electroplating and Assembly, Journal of Micromech. Microeng., Vol. 2 (1992), pp. 225–228.
18) Mohr, J., Bley, P., Strohrmann, M., Wallrabe, U., Microactuators Fabricated by the LIGA Process, Journal of Micromech. Microeng., Vol. 2 (1992), pp. 234–241.
19) Lehr, H., Ehrfeld, W., Schmidt, M., Kallenbach, E., Tuan., H., Application of the LIGA Technique for the Development of Microstructures Based on Electromagnetic Principles, Journal of Micromech. Microeng., Vol. 2 (1992), pp. 229–233.
20) Guckel, H., Christenson, T., Skorbis, K., Denton, D., Choi, B., Lovel, E., Lee, J., Bajikar, S., Chapman, T., Deep X-Ray and UV Lithographies for Micromechanics, Proceedings of the IEEE Solid-State Sensor and Actuator workshop Hilton Head SC (1990), pp. 118–122.
21) Frazier, B., Babb, J. W., Allen, M. G. and Taylor, D. G., Design and Fabrication of Electroplated Micromotors Structures, Proc of ASME Winter Annual Meeting, Atlanta, Vol. DSC-32 (1991), pp. 135–146.
22) Frazier, B. A., Allen, M. G., High Aspect Ratio Electroplated Microstructures Using A Photosensitive Polyimide Process, Proceedings of the IEEE Micro Electro Mechanical Systems, Travemunde, Germany (1992), pp. 87–92.
23) Engelmann, G., Ehrmann, O., Simon, J., Reichl, H., Fabrication of High Depth-to-Width Aspect Ratio Microstructures, Proceedings of the IEEE Micro Electro Mechanical Systems, Travemunde, Germany (1992), pp. 93–98.
24) Jacobs, P. F., Rapid Prototyping & Manufacturing: Fundamentals of Stereolithography, Society of Manufacturing Engineers in cooperation with the Computer and Automated Systems Association of SME (1992).
25) Miyagi, M., Yamazaki, H., Fujimori, S., Iwasawa, A. and Funakoshi, N., Multispiral Pregrooved Disk Fabricated by a Beam Scanning Method, Japanese Journal of Applied Physics, Vol. 29, No. 5 (1990), pp. L794–797.

26) Chitayat, A., Nanometer X-Y Positioning Stages for Scanning and Stepping, Journal of Vacuum Science and Technology B, Vol. 7, No. 6 (1989), pp. 1412–1417.
27) Ehrlich, D. J. and Tsao, J. Y., Laser Microfabrication - Thin Film Processes and Lithography, Academic Press Inc., (1989).
28) Yamaguchi, K., Nakamoto, T., Abraha, P., Mibu, S., 1994, The Accuracy of Micro-molds Produced by a UV Induced Polymerization, Transactions of the ASME Journal of Engineering for Industry, Vol. 116, August (1994), pp. 370–376.
29) Abraha, P., Nakamoto, T., Yamaguchi, K. and Karyawan, The Effect of Physical Parameters on the Fabrication of Microstructures by Photo Polymerization, Advancement of Intelligent Production, (1994), pp.564–569.
30) Yamaguchi, K., Nakamoto, T., Abraha, P., Manufacruring of High Aspect Ratio Micro Structures Using UV Sensitive Photopolymer, JSME International Series C, Vol. 39, No. 2 (1996), pp.387–396.
31) Nakamoto, T., Yamaguchi, K., Abraha, P. and Mishima, K., Manufacturing of Three-dimensional Micropart by UV Laser Induced Polymerization, Journal of Micromechanics and Microeng., Vol. 6, No. 2 (1996), pp. 240–253.
32) Linfoot, E. H., Recent Advances in Optics, Oxford at the Clarendon Press, (1955).
33) Sommerfelt, A., Optics, Academic Press Inc., New York (1954).
34) Yamada, T., Takato, N. and Kurokawa, T., A New Optical Circuit with a Steric Waveguide Pattern, Japanese Journal of Applied Physics, Vol. 22, No. 10 (1983), pp. L636–638.
35) Rubloff, G. W., Maskless Selected Area Processing, Journal of Vacuum Science and Technology B, Vol. 7, No.6 (1989), pp.1454–1461.
36) Kobayashi, K., Akiyama, K., Yoshizawa, I., Asakura, T., Laser-beam Scanning System Using an Acoustic-optic Deflector: Its Application to Fundus Imaging, Measurement Science and Technology, Vol. 1 (1990), pp. 151–157.
37) Hattori, K., Ikenaga, O., Wada, H., Tamamushi, S., Nishimura, E., Ikeda, N., Katoh, Y., Kusakabe, H., Yoshikawa, R., Takigawa, T., Triangular Shaped Beam Technique in EB Exposure System EX-7 for ULSI Pattern Formation, Japanese Journal of Applied Physics, Vol. 28, No. 10 (1989), pp. 2065–2069.